

# Long-Baseline Neutrino Experiment (LBNE) Project

Conceptual Design Report

Volume 1: The LBNE Project

March 10, 2012



# Contents

<b>Contents</b>	<b>i</b>
<b>List of Figures</b>	<b>iii</b>
<b>List of Tables</b>	<b>v</b>
<b>1 About the LBNE Conceptual Design Report</b>	<b>1</b>
<b>2 Executive Summary</b>	<b>3</b>
2.1 Introduction to the LBNE Project . . . . .	3
2.1.1 Scientific Motivation . . . . .	3
2.1.2 LBNE and the U.S. Neutrino-Physics Program . . . . .	4
2.1.3 Overview of Project Organization . . . . .	4
2.2 Overview of the LBNE Science Objectives . . . . .	5
2.3 Principal Parameters of the LBNE Project . . . . .	5
<b>3 LBNE Science Objectives</b>	<b>7</b>
<b>4 Project Organization</b>	<b>9</b>
4.1 Overview . . . . .	9
4.2 Work Breakdown Structure . . . . .	11
4.3 Project Cost and Schedule . . . . .	12
<b>5 Project Scope</b>	<b>13</b>
5.1 Overview . . . . .	13
5.2 Beamline at the Near Site . . . . .	14
5.3 Near Detector Complex . . . . .	15
5.4 Conventional Facilities at the Near Site . . . . .	16
5.5 Liquid Argon Far Detector . . . . .	18
5.6 Far Detector Depth . . . . .	21
5.7 Conventional Facilities at the Far Site . . . . .	21
<b>6 Experimental Capabilities</b>	<b>23</b>
6.1 Overview . . . . .	23
6.2 Accelerator-based Long-Baseline Neutrino Oscillations . . . . .	26
6.2.1 Measurements of Mass hierarchy and the CP Violating Phase . . . . .	27

6.2.2	Precision Measurements of the Oscillation Parameters in $\nu_\mu \rightarrow \nu_x$ Oscillations. . . . .	34
6.2.3	Observation of $\nu_\tau$ Appearance . . . . .	35
6.2.4	Resolving the $\theta_{23}$ octant . . . . .	38
6.2.5	Searches for New physics in Long Baseline Oscillations . . . . .	40
6.2.5.1	Non-standard Interactions . . . . .	40
6.2.5.2	Long Range Interactions . . . . .	42
6.2.5.3	Search for Active Sterile Neutrino Mixing . . . . .	42
6.3	Searches for Baryon Number Non-Conservation . . . . .	42
6.3.1	Proton Decay . . . . .	44
6.3.2	Nucleon/Anti-Nucleon Oscillations . . . . .	46
6.4	Supernova Burst Neutrinos . . . . .	47
6.5	Atmospheric Neutrinos . . . . .	49
6.6	Accelerator-based Short-Baseline Neutrino Oscillations . . . . .	52
6.7	Summary of Expected Measurements in LBNE . . . . .	56
<b>7</b>	<b>Supporting Documents</b>	<b>58</b>
	<b>References</b>	<b>61</b>

# List of Figures

4-1	LBNE Project Organization Chart . . . . .	10
5-1	Systems included in the LBNE Beamline subproject . . . . .	15
5-2	LBNE Near Site schematic longitudinal section view . . . . .	17
5-3	LBNE Overall Project Layout at Fermilab . . . . .	18
5-4	LAr-FD configuration within cavity . . . . .	19
5-5	TPC cross section view . . . . .	20
5-6	Schematic of underground conventional facilities for an LArTPC at the 4850L . . . . .	22
6-1	dE/dX from LArSoft . . . . .	25
6-2	Electron neutrino appearance probability at 1300km . . . . .	26
6-3	Event displays of beam interactions in an LArTPC . . . . .	29
6-4	Pi0 misid from the T2K 2km proposal . . . . .	31
6-5	Selection efficiencies of $\nu_e$ CC interactions in an LArTPC . . . . .	32
6-6	A complicated NC inelastic interaction in a LArTPC . . . . .	33
6-7	Resolution of electromagnetic showers from ICARUS [1] . . . . .	34
6-8	Event spectra of neutrino interactions in an LArTPC . . . . .	35
6-9	Measurements of MH, $\theta_{13}$ and $\delta_{cp}$ in a 34 kiloton LArTPC . . . . .	36
6-10	Precision measurements of $\sin^2 2\theta_{13}$ and $\delta_{cp}$ as a function of $\sin^2 2\theta_{13}$ . . . . .	37
6-11	Disappearance spectra in an LArTPC . . . . .	38
6-12	Fit to different values of $\Delta m_{32}^2$ and $\sin^2 2\theta_{23}$ . . . . .	38
6-13	Precision of the disappearance parameters as NC contamination varies . . . . .	39
6-14	$\nu_\tau$ appearance probability . . . . .	39
6-15	Event spectra of neutrino interactions in an LArTPC when $\theta_{23}$ is changed . . . . .	40
6-16	Sensitivity of LBNE to resolve the $\theta_{23}$ octant degeneracy . . . . .	41
6-17	Sensitivity to non-standard interactions . . . . .	43
6-18	Proton decay lifetime limits . . . . .	44
6-19	LArSoft simulation of $K^+ \rightarrow \mu^+ \rightarrow e^+$ decay in the MicroBooNE geometry . . . . .	45
6-20	Proton decay lifetime limit for $p \rightarrow K^+ \bar{\nu}$ as a function of time . . . . .	46
6-21	LArSoft simulated event, $p\bar{p}$ annihilation at rest . . . . .	47
6-22	SN burst event rates in 34-kt LArTPC . . . . .	48
6-23	Atmospheric neutrino spectrum . . . . .	49
6-24	Atmospheric neutrino oscillations vs zenith angle . . . . .	50
6-25	Zenith angle distributions of atmospheric neutrinos . . . . .	51
6-26	Sensitivities to the mass hierarchy and $\theta_{23}$ from atmospheric neutrinos. . . . .	52



# List of Tables

2-1	LBNE Principal Parameters . . . . .	6
4-1	WBS Chart (WBS Element Numbers and Names) to Level 3 . . . . .	11
4-2	Target Budget Cost Estimates at WBS Level 2 . . . . .	12
5-1	Depth requirement for a Liquid Argon TPC . . . . .	21
6-1	$\nu_\mu, \nu_\tau, \nu_e$ interaction rates per 100 kT.MW.yr ( $10^{21}$ protons-on-target) . . . . .	27
6-2	Range of detector efficiencies and background rejection based on handscan studies	28
6-3	Summary of LAr-TPC simulations . . . . .	30
6-4	Results for various event categories from hand scans . . . . .	32
6-5	Expected number of neutrino oscillation signal and background events at the LAr-FD . . . . .	33
6-6	Liquid argon efficiency and background numbers used for proton decay sensitivity calculations obtained from the paper by Bueno <i>et al.</i> [2]. . . . .	45
6-7	Supernova burst neutrino event rates for different models in 34 kt of LAr. . . . .	48
6-8	Estimated $\nu_\mu$ production rates water an argon target per ton for $1 \times 10^{20}$ POT at 459 m assuming neutrino cross section predictions from NUANCE [3] and a 120 GeV proton beam, 250 kA horn current, and a 2 m radius 250 m long decay region. Processes are defined at the initial neutrino interaction vertex and thus do not include final state effects. These estimates do not include detector efficiencies or acceptance [4,5]. . . . .	53
6-9	Expected measurement precision/sensitivities of long-baseline $\nu_\mu$ oscillation parameters in LBNE assuming an exposure of 34 kt LAr, 5+5 years $\nu + \bar{\nu}$ running at 708 kW. Values are quoted assuming a normal mass hierarchy. . . . .	56
6-10	Expected measurement precision/sensitivities using short-baseline $\nu_\mu$ interactions in the NDC, with an LAr and a 7 t FGT, assuming an exposure of 5+5 years $\nu + \bar{\nu}$ running at 708 kW. . . . .	57
7-1	LBNE CD-1 Documents . . . . .	58

# 1 About the LBNE Conceptual Design Report

[LABEL: “v1ch-about”]

The Long-Baseline Neutrino Experiment (LBNE) Conceptual Design Report (CDR) is intended to describe, at a conceptual level, the scope and design of the experimental and conventional facilities that the LBNE Project plans to build to address a defined set of neutrino-physics measurement objectives. The scope includes

- an intense neutrino beam aimed at a far site
- detectors located at the near site just downstream of the neutrino source
- a massive neutrino detector located at the far site
- construction of facilities at both the near and far sites

The selected near and far sites are Fermi National Accelerator Laboratory (Fermilab) and the Sanford Underground Laboratory at Homestake (Sanford Laboratory), respectively.

This CDR is organized into six stand-alone volumes, one to describe the overall LBNE Project and one for each of its component subprojects:

1. The LBNE Project
2. The Beamline at the Near Site
3. Detectors at the Near Site
4. The Liquid Argon Detector at the Far Site
5. Conventional Facilities at the Near Site
6. Conventional Facilities at the Far Site

1 Volume 1 is intended to provide readers of varying backgrounds an introduction to LBNE  
2 and to the following volumes of this CDR. It contains high-level information and refers the  
3 reader to topic-specific volumes and supporting documents, as appropriate. This volume  
4 briefly outlines the physics program that LBNE is designed to carry out. Readers desiring  
5 detailed information about the physics program and the experimental capabilities are referred  
6 to the LBNE Case Study Report (Liquid Argon TPC Detector) [6].

7 Each Volume 2 through 6 contains a common, brief introduction to the overall LBNE Project,  
8 an introduction to the individual subproject and a detailed description of its conceptual  
9 design.

10 The Project has chosen to separate out from the CDR a host of information related only  
11 indirectly to the design into a set of supporting documents. Detailed information on risk  
12 analysis and mitigation, value engineering, ES&H, costing, project management and other  
13 topics not directly in the design scope can be found in the documents listed in Chapter 7.

## 2 Executive Summary

### 2.1 Introduction to the LBNE Project

[LABEL: “sec:execsum”]

The Long-Baseline Neutrino Experiment (LBNE) Project team has prepared this Conceptual Design Report (CDR), which describes a world-class facility that will enable the scientific community to carry out a compelling research program in neutrino physics. The ultimate goal in the operation of the facility and experimental program is to measure fundamental physical parameters, explore physics beyond the Standard Model and better elucidate the nature of matter and antimatter.

#### 2.1.1 Scientific Motivation

Although the Standard Model of particle physics presents a remarkably accurate description of the elementary particles and their interactions, it is known that the current model is incomplete and that a more fundamental underlying theory must exist. Results from the last decade, that the three known types of neutrinos have nonzero mass, mix with one another and oscillate between generations, point to physics beyond the Standard Model.

A set of measurable quantities is associated with neutrino physics. The three-flavor-mixing scenario for neutrinos can be described by three mixing angles ( $\theta_{12}$ ,  $\theta_{23}$  and  $\theta_{13}$ ) and one CP-violating phase ( $\delta_{CP}$ ). The probability for neutrino oscillation also depends on the difference in the squares of the neutrino masses,  $\Delta m_{ij}^2 = m_i^2 - m_j^2$ ; three neutrinos implies two independent mass-squared differences ( $\Delta m_{21}^2$  and  $\Delta m_{32}^2$ ).

The entire complement of neutrino experiments to date has measured five of the mixing parameters: three angles,  $\theta_{12}$ ,  $\theta_{23}$ , and recently  $\theta_{13}$ , and two mass differences,  $\Delta m_{21}^2$  and  $\Delta m_{32}^2$ . The sign of  $\Delta m_{21}^2$  is known, but not that of  $\Delta m_{32}^2$ . The value of  $\theta_{13}$  has been determined to be much smaller than the other two mixing angles [?], implying that mixing is quantitatively different in the neutrino and quark sectors.

1 Observations of  $\nu_\mu \rightarrow \nu_e$  oscillations of a beam (composed initially of muon neutrinos,  $\nu_\mu$ )  
2 over a long baseline are the key to unambiguously determining the mass hierarchy (the sign of  
3  $\Delta m_{32}^2$ ), and the unknown CP-violating phase  $\delta_{cp}$ . The signature of CP violation is a difference  
4 in the probabilities for  $\nu_\mu \rightarrow \nu_e$  and  $\bar{\nu}_\mu \rightarrow \bar{\nu}_e$  transitions. The study of the disappearance of  
5  $\nu_\mu$  probes  $\theta_{23}$  and  $|\Delta m_{32}^2|$ . Non-standard physics can manifest itself in differences observed in  
6 higher precision measurements of  $\nu_\mu$  and  $\bar{\nu}_\mu$  disappearance over long baselines. The precision  
7 with which we know the current set of neutrino oscillation parameters ensures that the  
8 compelling physics program outlined is feasible with the combination of baseline, detector  
9 mass, and beam proposed for LBNE.

### 10 **2.1.2 LBNE and the U.S. Neutrino-Physics Program**

11 In its 2008 report, the Particle Physics Project Prioritization Panel (P5) recommended a  
12 world-class neutrino-physics program as a core component of the U.S. particle-physics pro-  
13 gram [7]. Included in the report is the long-term vision of a large detector in the Sanford  
14 Underground Laboratory in Lead, S.D., the site of the formerly proposed Deep Underground  
15 Science and Engineering Laboratory (DUSEL), and a high-intensity neutrino source at Fer-  
16 milab.

17 On January 8, 2010, the Department of Energy approved the Mission Need for a new long-  
18 baseline neutrino experiment that would enable this world-class program and firmly establish  
19 the U.S. as the leader in neutrino science. The LBNE Project is designed to meet this Mission  
20 Need. With the facilities provided by the LBNE Project, the LBNE Science Collaboration  
21 proposes to make unprecedentedly precise measurements of neutrino-oscillation parameters,  
22 including the value of the third mixing angle and the sign of the neutrino mass hierarchy.  
23 The ultimate goal of the program will be to search for CP-violation in the neutrino sector.  
24 A configuration of the LBNE facility, in which a large neutrino detector is located deep  
25 underground, could also provide opportunities for research in other areas of physics, such as  
26 nucleon decay and neutrino astrophysics, including studies of neutrino bursts from locally  
27 occurring supernovae. The scientific goals and capabilities of LBNE are summarized in al-  
28 phabet) Chapter 6 and fully described in the LBNE Case Study report for a Liquid Argon  
29 Time Projection Chamber (LArTPC) [6].

### 30 **2.1.3 Overview of Project Organization**

31 [LABEL: “v1-exsumm-projorg”]

32 The LBNE Project Office at Fermilab is headed by the Project Manager and assisted by the  
33 Project Engineer and Project Scientist. Project Office support staff include a Project Con-  
34 trols Manager and supporting staff, a Financial Manager, an ES&H Manager, a Computing  
35 Coordinator, QA and Risk Managers, a documentation team and administrative support.  
36 The Beamline, Liquid Argon TPC Detector and Conventional Facilities subprojects are man-

aged out of the Project Office at Fermilab, while the Near Detectors subproject is managed out of a Project Office at Los Alamos National Laboratory. More information on Project organization can be found in Chapter 4, and a full description of LBNE Project management is contained in The LBNE Project Management Plan [8].

## 2.2 Overview of the LBNE Science Objectives

The primary science objectives of the LBNE Project are the following experiments:

1. Search for, and precision measurements of, the parameters that govern  $\nu_\mu \rightarrow \nu_e$  oscillations. This includes precision measurement of the third mixing angle,  $\theta_{13}$ , and the CP-violating phase  $\delta_{CP}$  and determination of the mass ordering (the sign of  $\Delta m_{32}^2$ ).
2. Precision measurements of  $\theta_{23}$  and  $|\Delta m_{32}^2|$  in the  $\nu_\mu$  and  $\bar{\nu}_\mu$  disappearance channel.
3. Search for proton decay, yielding measurement of the partial lifetime of the proton ( $\tau/BR$ ) in one or more important candidate decay modes, e.g.  $p \rightarrow e^+\pi^0$  or  $p \rightarrow K^+\nu$ , or significant improvement in limits on it.
4. Detection and measurement of the neutrino flux from a core-collapse supernova within our galaxy, should one occur during the lifetime of LBNE.

A high-level discussion of these objectives plus a list of additional objectives that LBNE may pursue can be found in Chapter 3. The topics are covered thoroughly in the LBNE Case Study Report (Liquid Argon TPC Far Detector) [6]. and the 2010 Interim Report of the Long-Baseline Neutrino Experiment Collaboration Physics Working Groups [9].

## 2.3 Principal Parameters of the LBNE Project

The individual CDR volumes provide detail on the designs that LBNE has developed, based on a carefully constructed set of requirements that are organized in a traceable flow-down structure. Scientific requirements for LBNE, provided by the LBNE Collaboration, follow from the science objectives. Design of individual subprojects, systems and components are based on mid- and low-level requirements, respectively, that trace all the way back either to the science requirements or to LBNE's set of high-level programmatic requirements.

The experimental capabilities and performance of the far detector technology is documented thoroughly in the LBNE Case Study Report for a Liquid Argon TPC [10] and summarized in Chapter 6. Table 2-1 summarizes the performance metrics of the experiment.

**Table 2-1: LBNE Principal Parameters**  
**[LABEL: "table:param-summ-fd"]**

Project Element Parameter	Value
Near- to Far-Site Baseline	1,300 km
Primary Beam Power	708 kW, upgradable to 2.3 MW
Protons on Target per Year	$6.5 \times 10^{20}$
Primary Beam Energy	60 – 120 GeV (tunable)
Neutrino Beam Type	Horn-focused with decay volume
Neutrino Beam Energy Range	0.5 – 5 GeV
Neutrino Beam Decay Pipe Diameter $\times$ Length	4 m $\times$ 200 m
Near Site Neutrino Detector Type	Liquid Argon Time Projection Chamber (LArTPC) Tracker
Near Site Neutrino Detector Active Mass	2.5 ton
Far Detector Type	LArTPC
Far Detector Active (Fiducial) Mass	40 (34) kton
Far Detector Depth	1480 m

## 3 LBNE Science Objectives

[LABEL: “v1ch:sci-objectives”]

The LBNE science objectives are divided into three categories: *primary*, *secondary* and *additional secondary*. Our conceptual design by definition addresses the primary objectives. Secondary objectives are defined as those that may be enabled by the facility designed to achieve the primary objectives, i.e. with little or no impact on the cost or schedule. Achievement of the additional secondary objectives, in contrast, may require future upgrades to the facility designed to achieve the primary objectives.

The priorities for the scientific research to be enabled by the LBNE Project follow from the P5 recommendations, the Department of Energy (DOE) Mission Need Statement, discussions with the funding agencies (DOE Office of High Energy Physics (OHEP) and the Physics Division of the National Science Foundation), Fermilab management and the LBNE Science Collaboration.

The primary mission of the LBNE Project is to construct facilities that will enable observation of  $\nu_\mu \rightarrow \nu_e$  appearance over a distance (baseline) of greater than 1,000 km. At the LBNE baseline of 1300km, the magnitude of this signal is governed by the neutrino mass differences, the mass ordering, the CP-violating phase  $\delta_{cp}$ , and all three mixing angles  $\theta_{12}$ ,  $\theta_{23}$  and  $\theta_{13}$ . The different oscillation parameters impact the appearance spectrum differently at different neutrino energies and for neutrinos and anti-neutrinos. Therefore, precise measurement of  $\nu_\mu \rightarrow \nu_e$  and  $\bar{\nu}_\mu \rightarrow \bar{\nu}_e$  oscillations over a wide range of neutrino energies would allow for unambiguous determination of the neutrino mass ordering and mass differences, as well as precision measurements of  $\delta_{cp}$  and all 3 mixing angles. Measurement of this neutrino oscillation channel would also allow for research into CP violation in the neutrino sector, which is possibly connected to the dominance of matter over antimatter in the universe.

The entire set of LBNE science objectives is listed below.

### 1. Primary

- 1 (a) Search for, and precision measurements of, the parameters that govern  $\nu_\mu \rightarrow \nu_e$   
2 oscillations, as discussed above. This includes precision measurements of the third  
3 mixing angle,  $\theta_{13}$ , measurement of the CP violating phase  $\delta_{CP}$  and determination  
4 of the mass ordering (the sign of  $\Delta m_{32}^2$ ).
- 5 (b) Precision measurements of  $\theta_{23}$  and  $|\Delta m_{32}^2|$  in the  $\nu_\mu$ -disappearance channel.
- 6 (c) Search for proton decay, yielding measurement of the partial lifetime of the proton  
7 ( $\tau/\text{BR}$ ) in one or more important candidate decay modes, e.g.  $p \rightarrow e^+\pi^0$  or  
8  $p \rightarrow K^+\nu$ , or significant improvement in limits on it.
- 9 (d) Detection and measurement of the neutrino flux from a core-collapse supernova  
10 within our galaxy, should one occur during the lifetime of LBNE.

## 11 2. Secondary

- 12 (a) Other accelerator-based neutrino-oscillation measurements.
- 13 (b) Measurements of neutrino-oscillation phenomena using atmospheric neutrinos.
- 14 (c) Measurements of neutrino-oscillation phenomena and of solar physics using solar  
15 neutrinos.
- 16 (d) Measurement of other astrophysical phenomena using medium-energy neutrinos.
- 17 (e) Near detector studies of neutrino interactions.
- 18 (f) Near detector studies of nuclear and nucleon structure.
- 19 (g) Near detector searches for new physics.

## 20 3. Additional secondary

- 21 (a) Detection and measurement of the diffuse supernova-neutrino flux.
- 22 (b) Measurements of astrophysical and geophysical neutrinos of low energy.

## 4 Project Organization

[LABEL: “v1-proj-org”]

### 4.1 Overview

The LBNE Project consists of a set of subprojects, coordinated by a central Project Office located at Fermilab:

1. Project Management
2. Beamline
3. Near Detector Complex
4. (Obsolete)
5. Liquid Argon Far Detector
6. Conventional Facilities

As discussed in Section 2.1.3, the LBNE Project Office at Fermilab is headed by the Project Manager and assisted by the Project Engineer and Project Scientist. Project Office support staff include a Project Controls Manager and supporting staff, a Financial Manager, a Manager for Environment, Safety and Health (ES&H), a Computing Coordinator, Quality Assurance (QA) and Risk Managers, a documentation team and administrative support.

The Beamline, Liquid Argon Far Detector and Conventional Facilities subprojects are managed out of the Project Office at Fermilab, while the Near Detector Complex subproject is managed out of a Project Office at Los Alamos National Laboratory. A Project organization chart is shown in Figure 4-1.

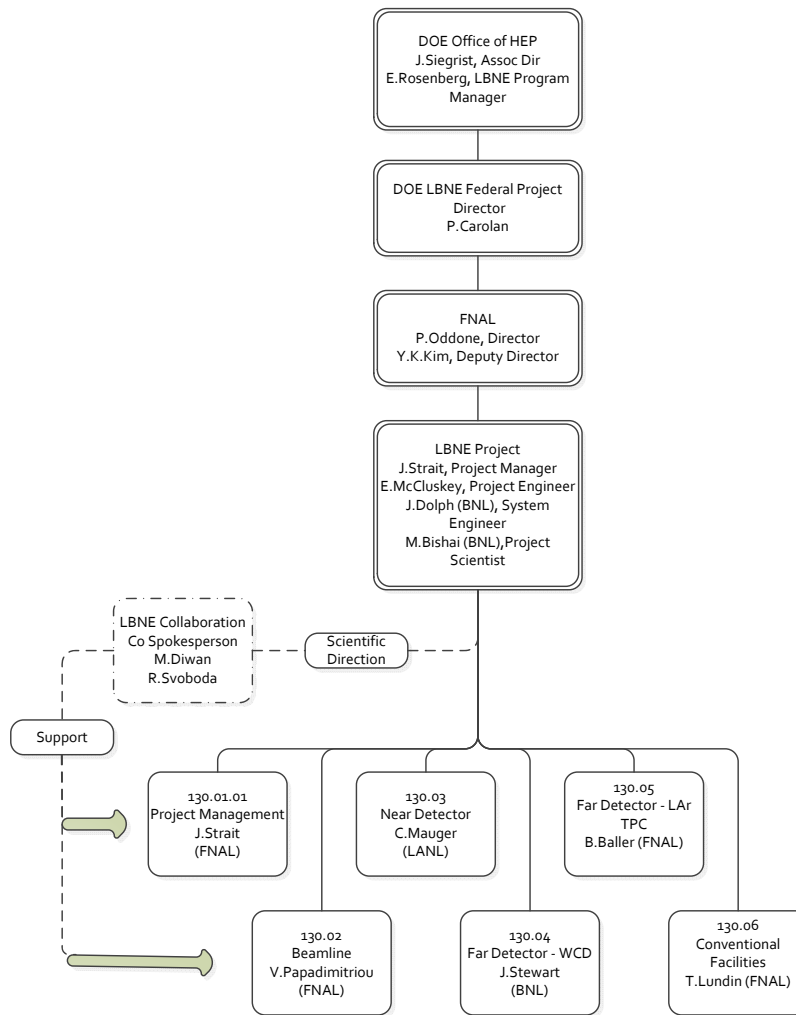


**Figure 4-1: LBNE Project Organization Chart**  
 [LABEL: "fig:org-chart"]

## 4.2 Work Breakdown Structure

The LBNE Work Breakdown Structure (WBS) is a means of organizing the work scope of the Project. A WBS decomposes the Project’s tasks and deliverables into smaller, manageable components. We define “LBNE” as WBS level 1, and each of its subprojects, listed above, as level 2. The subprojects, in turn, get broken out into lower, component levels. The following chart, shows the LBNE WBS down to level 3.

**Table 4–1:** WBS Chart (WBS Element Numbers and Names) [LABEL: “table:wbs-chart”]

Number	Name	Number	Name
130	LBNE		
130.01	LBNE Project Office	130.03.04	NDC – Neutrino Detectors
130.01.01	LBNE Conceptual Design	130.03.05	NDC – Detector Magnet
130.01.02	LBNE Preliminary Design	130.03.06	NDC – Global DAQ and Computing Systems
130.01.03	LBNE Final Design	130.05	Liquid Argon Far Detector (LAr)
130.01.04	LBNE Construction	130.05.01	LBNE LAr – Project Management
130.01.05	LBNE Closeout	130.05.02	LAr Cryogenics and Cryostat
130.02	Beamline	130.05.04	LAr Time Projection Chamber
130.02.01	Beamline – Project Management	130.05.05	LAr DAQ and Monitoring
130.02.02	Primary Beam		
130.02.03	Neutrino Beam	130.05.06	LAr Installation and Commissioning
130.02.04	Beamline – Systems Integration	130.05.07	LAr Photon Detector
130.03	Near Detector Complex (NDC)	130.05.09	LAr 1 kt Engineering Prototype
130.03.01	NDC – Project Management	130.06	Conventional Facilities (CF)
130.03.02	NDC – Measurement Strategy	130.06.01	CF – Project Management
130.03.03	NDC – Beamline Measurements	130.06.02	CF Near Site (Fermilab)
		130.06.04	CF Far Site (Sanford Lab)

**Table 4-2: Target Budget Cost Estimates at WBS Level 2**  
**[LABEL: "table:target-budget"]**

<b>WBS</b>	<b>Description</b>	<b>Budget Costs (in \$M)</b>
130.01	Project Management Office	
130.02	Beamline	
130.03	Near Detector	
130.05	LAr Far Detector	
130.06	Conventional Facilities	
Estimated Total Project Cost (TPC)		

1

## 2 **4.3 Project Cost and Schedule**

3 [LABEL: "sec:costsched"]

4 **FIXME:** *Add numbers*

5 The initial cost range of the LBNE Project is \$xxxM to xxxM, with a target total project  
 6 cost (TPC) for execution of \$xxxxM with contingency in at-year dollars. The initial schedule  
 7 range is xx years, beginning with CD-0 in January 2010. The target execution schedule is  
 8 xx years from CD-0 to CD-4.

# 5 Project Scope

[LABEL: “v1ch-scope”]

## 5.1 Overview

The DOE Mission Need for the LBNE Project proposes the following major elements:

- An intense neutrino beam aimed at a distant site
- A near-detector complex located near the neutrino source
- A suitably large neutrino detector located at the far site

The LBNE Project scope includes construction of experimental systems and facilities at two separate geographical locations. We present a reference design to achieve the Project’s mission in which a proton beam extracted from the Fermilab Main Injector (MI) is used to produce a neutrino beam. The neutrino beam traverses a near detector a few hundred meters downstream before traveling through the Earth’s mantle to a far detector located 1,300 km away in the Sanford Underground Laboratory, the site of the former Homestake Mine in Lead, South Dakota. The 1,300-km separation between the sites presents an optimal baseline for LBNE’s neutrino-oscillation physics goals.

The main scope elements on the Fermilab site, also referred to as the Near Site, include:

- Magnets and support equipment to transport the extracted protons to the target (where approximately 85% of them interact, producing pions and kaons)
- A target and target hall **FIXME:** *called target complex?*
- Magnetic focusing horns to direct pions and kaons into a decay tunnel

- 1     • A decay tunnel where these particles decay into neutrinos
- 2     • A beam absorber at the end of the decay tunnel to absorb the residual secondary  
3       particles
- 4     • Near detectors to make beamline measurements and neutrino-flux and spectrum mea-  
5       surements
- 6     • Conventional facilities at Fermilab to support the technical components of the primary  
7       proton beam, the neutrino beam and the near detectors

8 The main scope elements at the Sanford Laboratory site, the Far Site, include:

- 9     • The massive far detector, located underground
- 10    • Infrastructure required for the far detector, both above- and below-ground
- 11    • Conventional facilities at Sanford Laboratory to house and support the technical com-  
12      ponents of the far detector

## 13 5.2 Beamline at the Near Site

14 The LBNE beamline complex at Fermilab will be designed to provide a neutrino beam of  
15 sufficient intensity and energy to meet the goals of the LBNE experiment with respect to  
16 long-baseline neutrino-oscillation physics. The design is that of a conventional, horn-focused  
17 neutrino beamline. The components of the beamline will be designed to extract a proton  
18 beam from the Fermilab Main Injector and transport it to a target area where the collisions  
19 generate a beam of charged particles. This secondary beam, aimed toward the far detector, is  
20 followed by a decay-pipe tunnel where the particles of the secondary beam decay to generate  
21 the neutrino beam. At the end of the decay pipe, an absorber pile removes the residual  
22 particles.

23 The facility is designed for initial operation at proton beam power of 700 kW, **FIXME:** *not*  
24 *708?* with the capability to support an upgrade to 2.3 MW. In our reference design, extraction  
25 of the proton beam occurs at MI-10, a new installation. After extraction, this primary beam  
26 follows a straight compass heading to the far detector, but will be bent vertically upward  
27 for approximately 700 feet before being bent vertically downward at the appropriate angle,  
28 0.1 radian (5.6°), as shown in Figure 5-1. The primary beam will be above grade for most  
29 of its length.

30 The target marks the transition from the intense, narrowly directed proton beam to the  
31 more diffuse, secondary beam of particles that in turn decay to produce the neutrino beam.

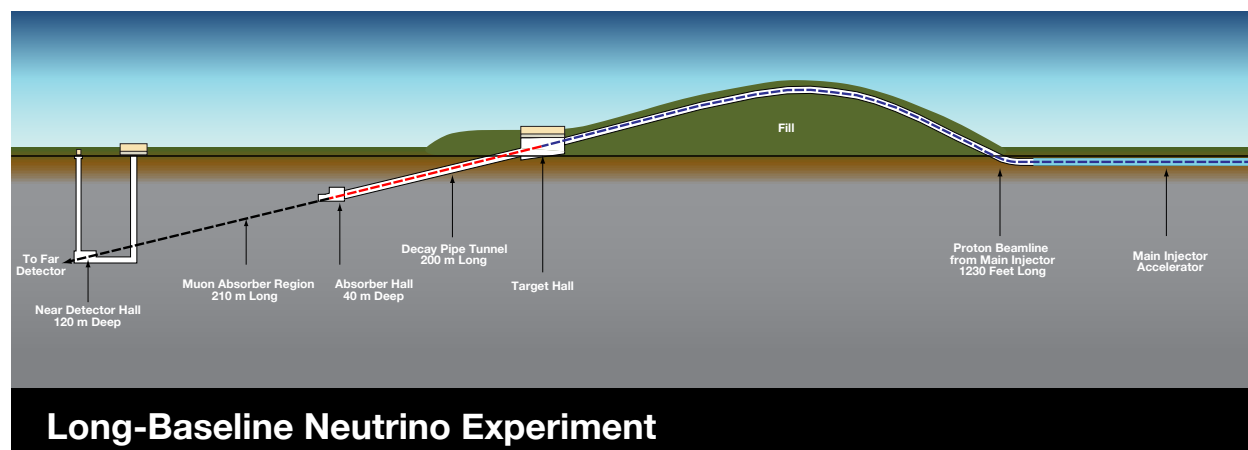


**Figure 5–1:** Schematic of the systems included in the LBNE Beamline subproject. The top of the engineered hill is 22 m above grade, somewhat less than half the height of Wilson Hall, shown on the right in the distance.

[LABEL: “fig:mi10\_beam\_schem”]

1 The interaction of a single proton in the target creates, on average, four charged particles  
 2 consisting mostly of pions and kaons. These secondary particles are short-lived. Each sec-  
 3 ondary particle decay generates a muon, which penetrates deep into the surrounding rock  
 4 and a neutrino that continues on toward the near and far detectors.

5 After collection and focusing, the pions and kaons that did not initially decay – the residual  
 6 particles mentioned above – need a long, unobstructed volume in which to decay. This decay  
 7 volume in the LBNE reference design is a pipe of circular cross section with its diameter and  
 8 length optimized such that decays of the pions and kaons result in neutrinos in the energy  
 9 range useful for the experiment.

### 10 5.3 Near Detector Complex

11 The LBNE Near Detector Complex (NDC), located downstream of the target, consists of two  
 12 detector systems, one for making measurements of muons in the beamline and the other to  
 13 measure the neutrino spectrum, interactions and kinematics. The NDC’s primary purpose is  
 14 to maximize the oscillation physics potential of the far detector. The scope and design of the  
 15 ND are therefore driven by the overall experiment’s requirements for the neutrino-oscillation  
 16 analysis, which will not yet be known precisely by CD-1. In general however, the ND must: (1)  
 17 measure the intrinsic  $\nu_e$  component of the beam with sufficient precision to allow subtraction  
 18 of this irreducible background, and (2) measure the detailed final state kinematics of neutrino  
 19 interactions of the LBNE beam on argon nuclear targets with sufficient precision to allow  
 20 prediction of the particle identification efficiency in the far detector.

1 The Beamline Measurements system will be placed in the region of the absorber at the  
2 downstream end of the decay region. Three detector systems will be deployed to measure  
3 (a) the muon-beam profile (with a grid of ion chambers), (b) the muon-beam energy spec-  
4 trum (using variable-pressure threshold gas Cherenkov detectors), and (c) the muon flux (by  
5 counting the number of muon-decay Michel electrons in “stopped-muon detectors”). These  
6 measurements constrain the beam neutrino flux and are used in conjunction with the near  
7 detector measurements to extract more detailed information on neutrino cross-sections and  
8 final state interactions.

9 The Neutrino Measurements system will be placed underground in the Near Detector Hall  
10 450 m downstream of the target. The reference design consists of time projection chamber  
11 tracker (LArTPCT), based on the MicroBooNE design. It is surrounded by a magnet in order  
12 to distinguish the charge-sign of muon (anti)neutrino interactions. The LArTPCT will use  
13 the UA-1 magnet design, **FIXME:** *need reference* interspersed with resistive-plate chambers  
14 (RPC) for muon identification.

## 15 5.4 Conventional Facilities at the Near Site

16 The baseline design for the LBNE Project at the Near Site incorporates extraction of a  
17 proton beam from the MI-10 point of the Main Injector, which then determines the location  
18 of the NDC and supporting Near Site Conventional Facilities. The Near Site Conventional  
19 Facilities not only provide the support buildings for the underground facilities, but also  
20 provide the infrastructure to direct the beamline from the below-grade extraction point to  
21 the above-grade target. See Figure 5-1 for a schematic of the experimental and conventional  
22 Near Site facilities.

23 Figure 5-2 shows a schematic longitudinal section of the entire Near Site, with an exaggerated  
24 vertical scale of 3 to 1 to show the entire Project alignment in one illustration.

25 The beam will travel approximately 1,200 ft (366 m) through the proposed Primary Beamline  
26 Enclosure to the Target Hall **FIXME:** *complex?* and through focusing horns and a target  
27 to create an intense neutrino beam that will be directed through a 656-ft (200-m) long decay  
28 pipe through a hadron absorber where the beam will then leave the Absorber Hall and  
29 travel 689 ft (210 m) through bedrock to the NDC, to range out (absorb) muons, before  
30 reaching the Near Detector Hall. The neutrino beam will then pass through the NDC before  
31 continuing through the Earth’s mantle to the Far Site.

32 The Near Site Conventional Facilities LBNE Project layout at Fermilab, the “Near Site”, is  
33 shown in Figure 5-3. Following the beam from east to west, or from right to left in this fig-  
34 ure, is the underground Primary Beamline Extraction Enclosure, the underground Primary  
35 Beamline Enclosure/Pre-target Tunnel and its accompanying surface based Service Building  
36 (LBNE 5), the in-the-berm Target Complex (LBNE 20), the Decay Pipe, the underground

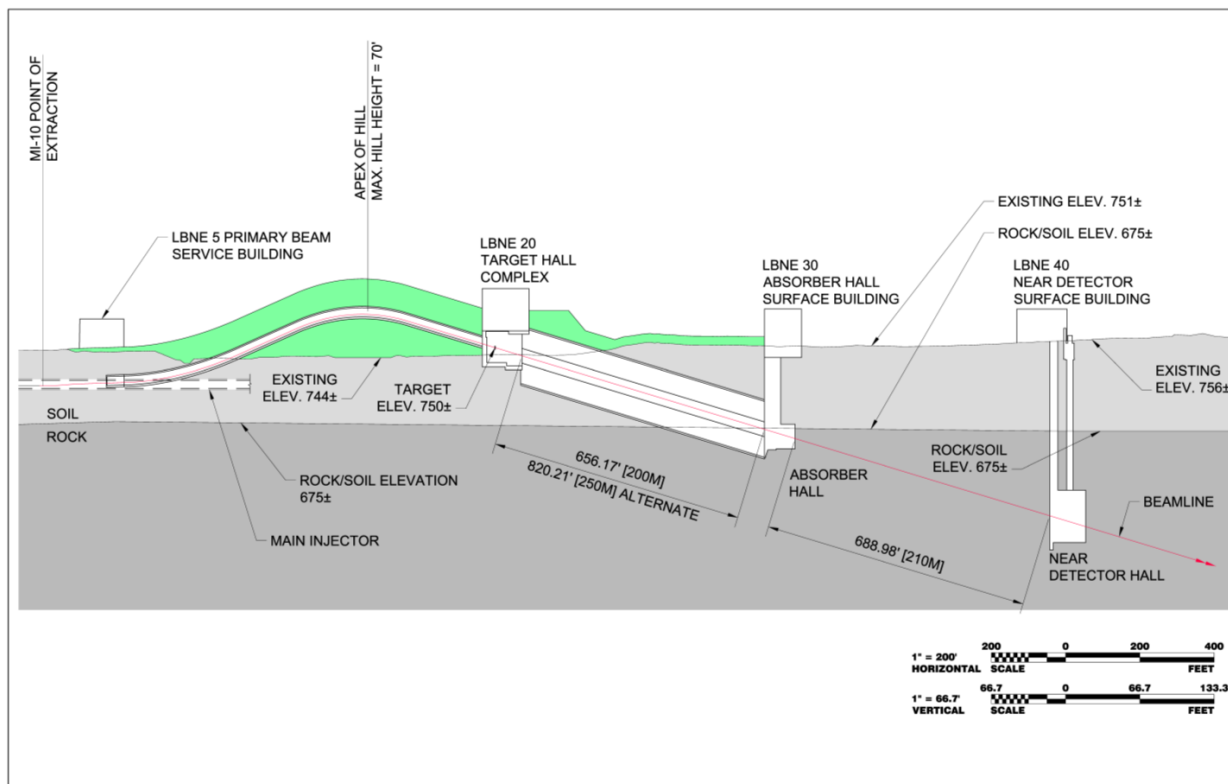


Figure 5-2: LBNE Near Site schematic longitudinal section view  
 [LABEL: "fig:10\_nscf\_schem"]

- 1 Absorber Hall and its surface Service Building (LBNE 30), and the underground Near De-  
 2 tector Hall and its surface Service Building (LBNE 40). The Project limits are bounded by  
 3 Giese Road to the north, Kautz Road to the east, Main Injector Road to the south, and  
 4 Kirk Road to the west.



Figure 5-3: LBNE Overall Project Layout at Fermilab  
 [LABEL: "fig:nscf\_layout"]

- 5 These facilities are described in detail in Volume 5 of this CDR.

## 6 5.5 Liquid Argon Far Detector

- 7 The LBNE far detector is being designed as a liquid argon time projection chamber (LArTPC).  
 8 LArTPCs combine fine-grain tracking with total absorption calorimetry to enable precision  
 9 neutrino-event detection in scalable neutrino detectors. The millimeter-scale spatial resolu-  
 10 tion combined with recordable  $dE/dx$  provides excellent signal efficiency and background  
 11 rejection for both beam and non-beam neutrino physics.

1 The LArTPC detector technology is relatively simple. The signal is generated by a well  
2 known electromagnetic process, the generation of ionization electrons by the passage of  
3 particles through liquid argon. The fraction of electrons that recombine and the trajectory  
4 of the electrons are determined by the electric field in the drift region.

5 The LBNE LArTPC detector, called LAr-FD, will be configured as two cryostats, each a  
6 rectangular vessel 24 m wide, 16.0 m high and 49.0 m long, of active mass 20 kt and fiducial  
7 mass of 17 kt. **FIXME:** *define these terms* They will be arranged end-to-end in a single  
8 cavity, separated by a 15-m clear space within thick septum walls, with a the long axis  
9 oriented along the incoming beam. The LAr-FD will be housed at 4,850 feet underground  
10 (referred to as the 4850L). Its configuration is illustrated in Figure 5-4.

11 The detector includes a cryogenic system that keeps the liquid argon at a temperature of  
12 89 K and maintains the required purity using a pump and filter system.

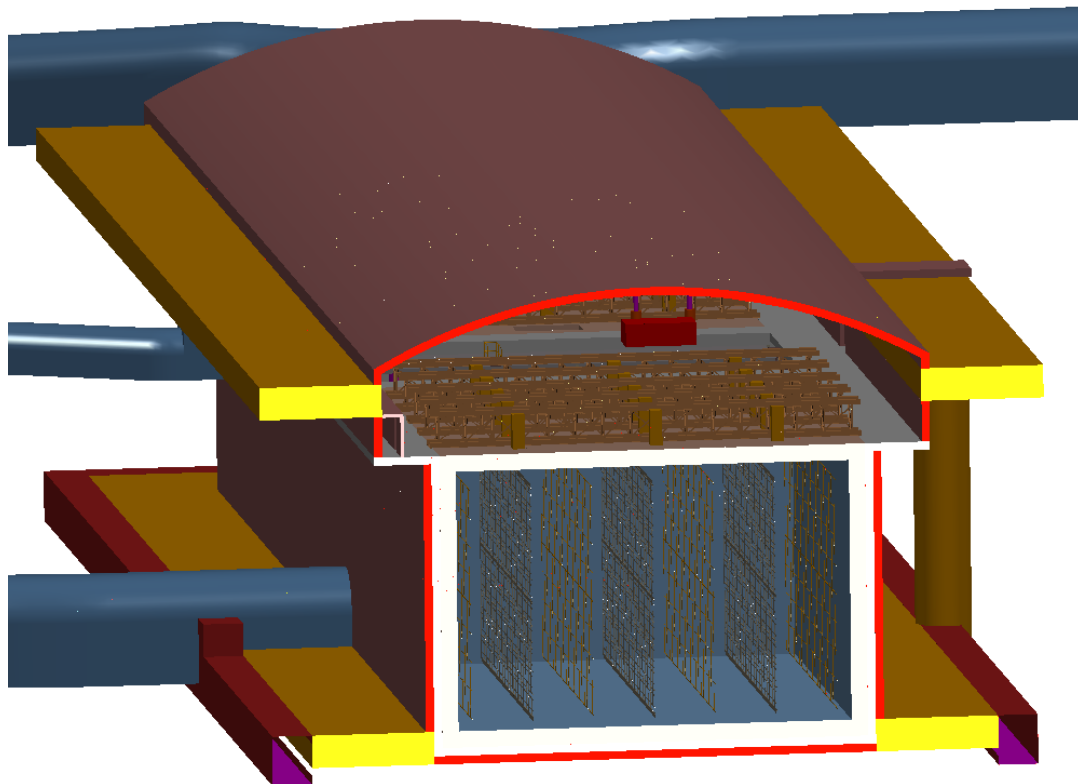


**Figure 5-4:** LAr-FD configuration within cavity  
[LABEL: "fig:lar40-cavern"]

- 1 The detection system in each cryostat consists of a time projection chamber (TPC) and  
 2 readout electronics. A TPC consists of rows of cathode planes interleaved with rows of anode  
 3 planes between sets of which uniform electric fields are created. See Figure 5-5. Charged  
 4 particles passing through the TPC release ionization electrons that drift along the field to  
 5 the anode planes. The bias voltage is set on the anode wires (of which there are four layers)  
 6 such that ionization electrons drift between the first several layers (called *induction* layers)  
 7 and are collected on the last layer (the *collection* layer).

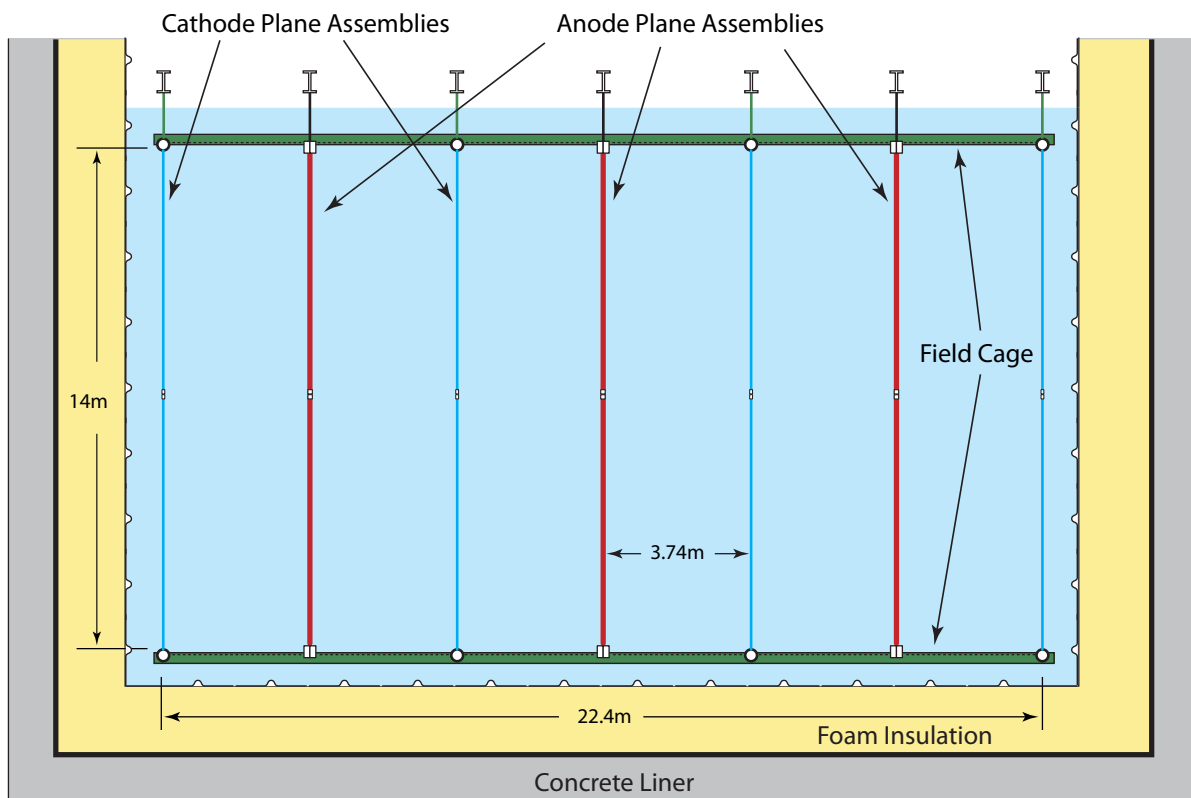


**Figure 5-5:** TPC cross section view  
 [LABEL: "fig:lar40-tpc-xsect"]

- 8 Readout electronics amplify and continuously digitize the induced waveforms on the sensing  
 9 wires at several MHz, and transmit these data to the data acquisition (DAQ) system. The  
 10 wire layers are oriented at different angles relative to each other allowing a 3D reconstruction  
 11 of the particle trajectories.

## 5.6 Far Detector Depth

In 2008, the LBNE Science Collaboration undertook a detailed study of the depth requirements for the main physics topics of interest with large detectors. This work is referred to as “The Depth Document” [11]. The topics considered were accelerator-generated neutrinos; supernova, solar and atmospheric neutrinos; and nucleon decay. The requirement on the depth of the detector is guided by the rate of the desired signals and the rate of backgrounds from cosmic rays over a very wide range of energies (from solar-neutrino energies of 5 MeV to high energies in the range of hundreds of GeV.)

Table 5-1 lists the depth requirements for this detector to accomplish LBNE’s goals for each physics measurement.

**Table 5-1:** Depth requirement (in meters-water-equivalent) by physics topic for a Liquid Argon TPC

[LABEL: “table:depth-lar”]

Physics Topic	Depth (mwe)
Long-baseline accelerator	0 – 1,000
$p \rightarrow K^+ \nu$	> 3,000
Day/Night ${}^8\text{B}$ Solar $\nu$	$\sim 4,300$
Supernova burst	3,500
Relic supernova $\nu$	> 2,500
Atmospheric $\nu$	2,400

## 5.7 Conventional Facilities at the Far Site

The Far Site used in our reference design is the Sanford Underground Laboratory at Homestake, in Lead, S.D.

The scope of the underground facilities required for the LAr includes new excavated spaces at the 4850L for the detector, utility spaces for experimental equipment, utility spaces for facility equipment, drifts for access, Area of Refuge (AoR) for emergencies, as well as construction-required spaces. Underground infrastructure for the facility includes power to experimental equipment, domestic water, industrial water for process and fire suppression, ventilation and exhaust, fire detection and alarm, normal and standby power systems, sump pump drainage system for conveying native infiltration water to the facility-wide pump discharge system, and cyberinfrastructure for communications and security. In addition, existing infrastructure that must be upgraded to meet LBNE needs include rehabilitation of the Ross and Yates Shafts from the surface down to the 4850L. Rehabilitation of the Ross Shaft is scheduled



# 6 Experimental Capabilities

[LABEL: “ch:lar-detperf”]

## 6.1 Overview

The primary science objectives for LBNE as described in chapter 3 dictate the need for very large mass, 100 kilo-ton scale neutrino detectors located at large depth at a distance of > 1000km from the neutrino source at Fermilab. A large mass is required to accumulate enough neutrino interactions -  $\mathcal{O}(1000)$  events - for precision measurements of the parameters that govern  $\nu_\mu \rightarrow \nu_e$  oscillations as well as providing sufficient nucleons to enable the search for proton decay. The detector needs to be located at large depths [11] to reduce backgrounds to a sufficient level for low energy physics searches such as proton decay and supernova neutrinos. To meet both the primary and secondary physics objectives, the detector is required to have excellent particle identification over a wide range of particle energies from a few GeV (for measuring long baseline beam neutrino oscillations and atmospheric neutrinos) to a few MeV (for identification of supernova, solar and geophysical neutrinos).

Neutrino events detected in experiments like LBNE are often categorized according the particle mediating the interaction. The term (used below, and throughout this document) “neutral current process” (NC) refers to an interaction which is mediated by the neutral boson  $Z^0$ . Similarly, a “charged current” (CC) interaction involves a positive or negative charged W boson. The flavor of a neutrino in a CC interaction is tagged by the flavor of the emitted lepton:  $e, \mu, \tau$  tag  $\nu_e, \nu_\mu, \nu_\tau$  interactions. CC and NC interactions of neutrinos with energies > 1 GeV are inelastic and the target nucleus disintegrates producing multiple hadrons. A large component of the background for  $\nu_e$  CC interactions is from NC interactions where a  $\pi^0$  is produced. The  $\pi^0$  decays to 2  $\gamma$ s which shower electromagnetically and fake electrons. NC interaction interactions where a charged pion is produced are also the predominant background for  $\nu_\mu$  CC interactions where the pion fakes a muon. Therefore to study neutrino flavor oscillations with high precision, the LBNE far detector has to have high efficiency, high purity  $e/\mu/\gamma$  and  $\pi/K/p$  separation. A “quasi-elastic” (QE) event is a

1 CC event in which the scattering of the neutrino is almost elastic with only a charged lep-  
2 ton and a nucleon or nucleons emerging from the target nucleus. The charged lepton in QE  
3 events carries most of the energy of the neutrino, as a result QE interactions have the best  
4 neutrino energy resolution. Precision tracking of protons from neutrino interactions improves  
5 CC/NC separation and the neutrino energy resolution. Final State Interactions (FSI) inside  
6 the nucleus will alter the expected nucleon types and spectrum, and measurement of this  
7 effect is a major goal of the Near Detector.

8 A massive liquid Argon TPC has been chosen as the far detector technology for the LBNE  
9 project. TPCs are the detectors of choice for low rate, large volume, high precision particle  
10 physics experiments due to their excellent 3D position resolutions and particle identification  
11 in large volumes. In addition to detailed event topologies and measurements of particle kine-  
12 matics,  $dE/dx$  measurements allow TPCs to unambiguously distinguish electrons, muons,  
13 photons, kaons, pions and protons (see Figure 6-1) over a wide range of energies.

14 A massive Liquid Argon TPC with a fiducial volume of 34kT as the LBNE far detector  
15 fulfills the high mass requirement coupled with the excellent particle identification over a  
16 wide range of energies expected from a large volume TPC. The photo-detection system will  
17 detect scintillation light in order to: (1) determine the exact time of the start of the drift  
18 process, and (2) provide a trigger for the proton decay, supernova, and other non-beam  
19 physics. The large mass and the location of the LBNE Liquid Argon TPC at the 4850ft  
20 level of the Homestake Mine enables searches for beyond the Standard Model Processes  
21 predicted by several grand unified theories such as proton decay and nucleon anti-nucleon  
22 oscillations. In particular, the identification of kaons with high purity in a TPC enables  
23 measurements of proton decays with a charged kaon in the final state. The high mass and  
24 timing resolution of the detector enable detailed energy and time dependent measurements  
25 of Supernova burst neutrinos, should one occur within our Galaxy. Atmospheric and beam  
26 neutrinos share the same requirements for particle identification, but atmospheric neutrinos  
27 provide an independent sample of neutrinos oscillating over much longer distances. Solar  
28 neutrinos require very low thresholds ( $< 10$  MeV) which could be achieved if radioactive  
29 contaminants in the TPC can be minimized.

30 The LBNE project includes a near-detector complex located near the neutrino source whose  
31 primary purpose is to measure the un-oscillated rate of beam neutrinos with high precision.  
32 The combination of high precision neutrino beam-line measurements, high intensity wide-  
33 band neutrino beam and a high resolution near detector will also enable the near detector  
34 complex to carry out a rich program of short baseline neutrino physics. The wide-band  
35 on-axis beam coupled with independent measurements of the neutrino flux at the source  
36 enabled by the secondary beam-line instrumentation will enable the high resolution ND to  
37 outperform current short baseline experiments.

38 In this chapter, we present a summary of the experimental capabilities and performance  
39 metrics of LBNE. The “Fall 2010 Report from the Physics Working Group” [9] has a detailed  
40 study of the extensive physics capabilities of LBNE. The LBNE Case Study Report for a

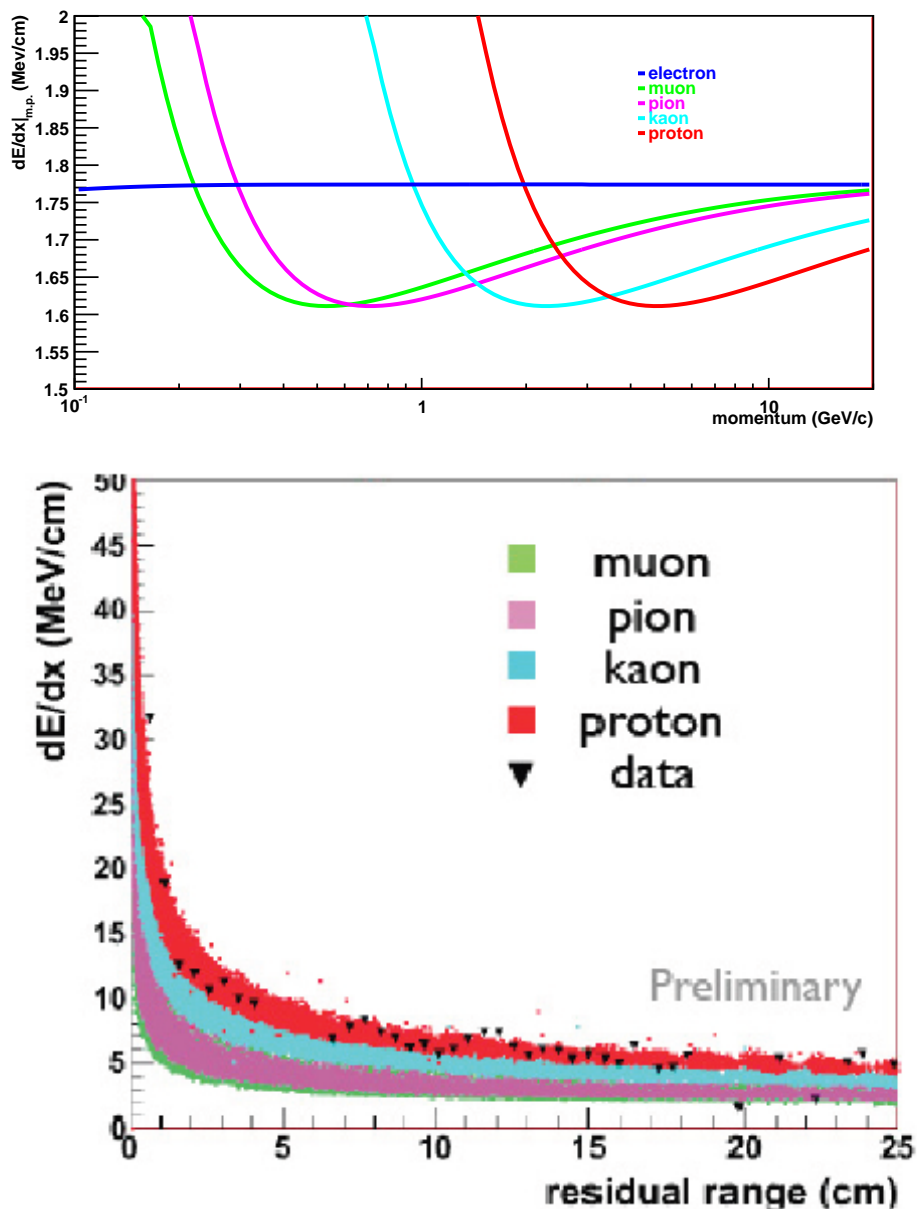


**Figure 6-1:** Distributions of  $dE/dX$  values for different charged particle species from a GEANT4 simulation of a liquid Argon TPC. The top plot is the most probable value of  $dE/dX$  vs particle momentum. The bottom plot is the value of  $dE/dX$  versus residual range from a GEANT4 simulation. The points are proton  $dE/dX$  measurements obtained from ArgoNEUT.

[LABEL: "fig:dedx-tpc"]

1 Liquid Argon TPC [10] has further details on the performance metrics of the LAr-TPC.

## 2 6.2 Accelerator-based Long-Baseline Neutrino Oscillations

3 The primary scientific objective for LBNE is the precision measurement of the parameters  
 4 that govern neutrino oscillations over a long baseline exceeding 1000km. The observation  
 5 and measurement of the characteristics of  $\nu_\mu/\bar{\nu}_\mu \rightarrow \nu_e/\bar{\nu}_e$  oscillations in the neutrino energy  
 6 region from 0.2 to 6 GeV at 1300km would enable the unambiguous determination of the  
 7 neutrino mass hierarchy and the measurement of  $\delta_{cp}$ , the CP phase. The  $\nu_\mu \rightarrow \nu_e$  oscillation  
 8 probability (colored curves) at 1300km for  $\sin^2 2\theta_{13} = 0.1$  and various values of the CP  
 9 violating phase  $\delta_{cp}$  are shown in Figure 6-2. The shaded histogram is the unoscillated  $\nu_\mu$   
 10 CC spectrum at 1300km obtained from the LBNE conceptual beam design where the first  
 11 focusing horn design has been further optimized to maximize the rate of  $\nu_e$ s appearing at the  
 12 far detector. This beam design assumes a 250m decay volume, which is under consideration  
 13 for LBNE.

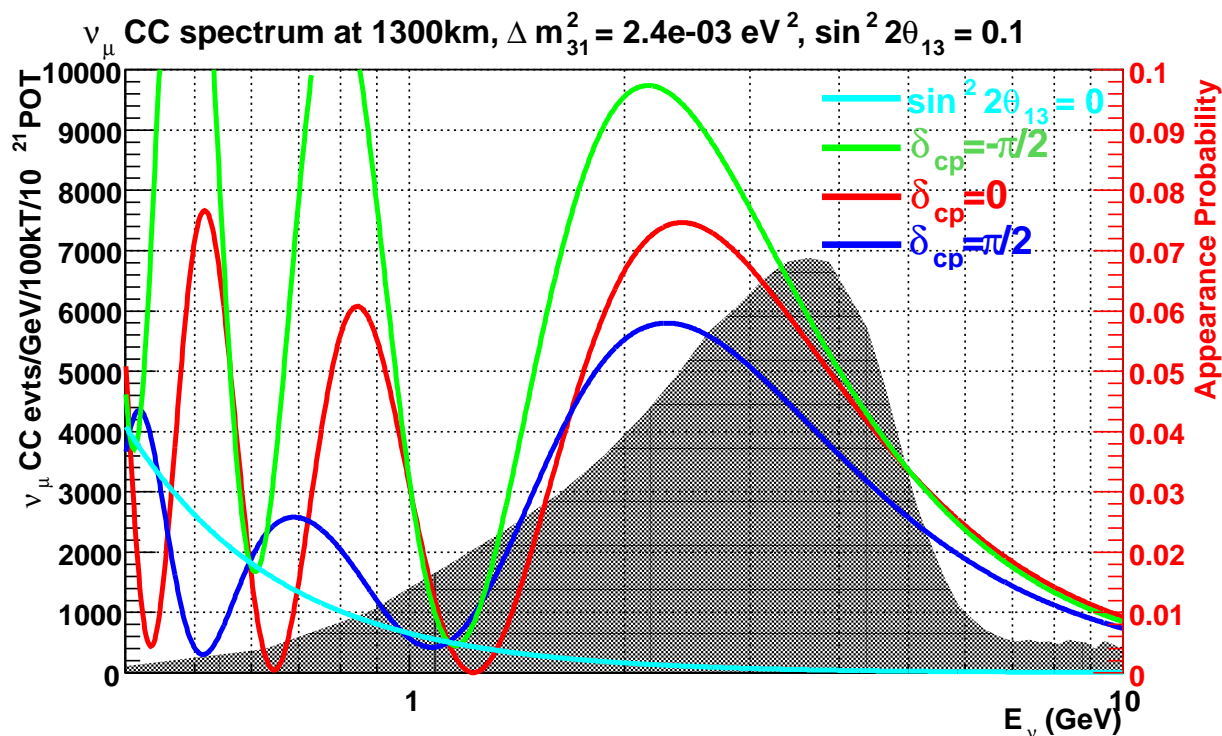


**Figure 6-2:** The  $\nu_\mu \rightarrow \nu_e$  oscillation probability (colored curves) at 1300km for  $\sin^2 2\theta_{13} = 0.1$  and various values of the CP violating phase  $\delta_{cp}$ . The shaded histogram is the unoscillated  $\nu_\mu$  CC spectrum at 1300km from the low-energy (LE) beam tune. This beam tune includes a 250m decay pipe and further optimization of LBNE horn 1 and target designs.

[LABEL: "fig:proboverlay1"]

1 In Table 6–1, the neutrino interaction rates for all 3 known species of neutrinos as expected  
 2 at the LBNE far detector site are listed. We have assumed a tunable beam spectrum obtained  
 3 by changing the distance between the target and the optimized horn 1 design.

Target Position	$\nu_\mu$ CC	$\nu_\mu$ CC osc	$\nu_\mu$ NC	$\nu_e$ CC beam	$\nu_\mu \rightarrow \nu_e$ CC	$\nu_\mu \rightarrow \nu_\tau$ CC
-0.3 m (LE tune)	29K	11K	4.1K	260	1300	140
-1.5 m (ME tune)	44K	28K	8.4K	320	1100	640
-2.5 m (HE tune)	47K	35L	9.6K	280	770	800

**Table 6–1:**  $\nu_\mu, \nu_\tau, \nu_e$  interaction rates per 100 kT.MW.yr ( $10^{21}$  protons-on-target) at the far detector site in LBNE for different beam tunes obtained by moving the target w.r.t. horn 1. Normal hierarchy,  $\sin^2 2\theta_{13} = 0.1$ . The rates are integrated in the region 0.5–20 GeV. The first column of numbers is the unoscillated  $\nu_\mu$  total charge-current interaction rate. The second column of numbers is the rate of  $\nu_\mu$  CC interactions expected given  $\nu_\mu \rightarrow \nu_\mu$  oscillations.

[LABEL: “tab:lbl\_event\_rates”]

#### 4 6.2.1 Measurements of Mass hierarchy and the CP Violating Phase

5 A primary science objective of LBNE is to make precise measurements of the parameters that  
 6 govern  $\nu_\mu \rightarrow \nu_e$  oscillations. These parameters probe CP violation in the neutrino sector  
 7 and determine the neutrino mass hierarchy. The sensitivity of the LAr-FD for  $\nu_e$  appearance  
 8 physics is primarily dependent on the signal efficiency for detecting electron-neutrino inter-  
 9 actions and the background rejection of neutral current (NC) events and  $\nu_\mu$  charged current  
 10 (CC) events in the range of 200MeV to 6 GeV. NC events containing  $\pi^0$ s are the dominant  
 11 source of background from NC interactions. The  $\pi^0$  decays to two photons which convert to  
 12  $e^+e^-$  pairs and initiate an electromagnetic shower that can be difficult to distinguish from  
 13 an electron shower. High efficiency and purity  $e/\gamma$  separation is required to distinguish  $\nu_e$   
 14 CC from  $\nu$  NC events. Excellent  $\mu/e$  separation is also required to enable the distinction  
 15 of  $\nu_\mu$  and  $\nu_e$  CC interactions. In addition to measurements of the CP parameters, LBNE  
 16 will search for physics beyond the standard model with high precision measurements of the  
 17 parameters  $\Delta m_{32}^2$  and  $\sin^2 2\theta_{23}$  in  $\nu_\mu$  and  $\bar{\nu}_\mu$  long baseline oscillations. These measurements  
 18 require high purity identification of  $\nu_\mu$  CC interactions for which high precision separation  
 19 of  $\mu/\pi/p^+$  separation is necessary. The strength of the LAr-FD is the ability to use detailed  
 20 event topology, particle kinematics, and dE/dX to differentiate  $\nu_e, \nu_\mu$  CC and NC  $\pi^0$  event  
 21 classes with high purity and efficiency as illustrated in Figure 6–3.

22 The expected performance of the LBNE FD LAr-TPC is extrapolated from the analysis  
 23 results obtained from four independent studies of massive LAr-TPCs. The four studies are  
 24 detailed in references [12] [13] [14] [15] and are summarized in Table 6–3.

25 The most detailed LAr TPC performance parameters we have to date were obtained from  
 26 studies by the ICARUS collaboration and the 2km detector proposal for the T2K experiment

**Table 6–2:** Estimated range of the LAr-TPC detector performance parameters for the primary oscillation physics. Signal efficiencies, background levels, and resolutions are obtained from the studies described in this chapter (middle column) and the value chosen for the baseline LBNE neutrino-oscillation sensitivity calculations (right column). \* For atmospheric neutrinos this is the mis-identification rate for  $< 2$  GeV events, the mis-identification rate is taken to be 0 for  $> 2$  GeV.

Parameter	Range of Values	Value Used for LBNE Sensitivities
For $\nu_e$ CC appearance studies		
$\nu_e$ CC efficiency	70-95%	80%
$\nu_\mu$ NC mis-identification rate	0.4-2.0%	1%
$\nu_\mu$ CC mis-identification rate	0.5-2.0%	1%
Other background	0%	0%
Signal normalization error	1-5%	1%
Background normalization error	2-10%	5%
For $\nu_\mu$ CC disappearance studies		
$\nu_\mu$ CC efficiency	80-95%	85%
$\nu_\mu$ NC mis-identification rate	0.5-10%	0.5%
Other background	0%	0%
Signal normalization error	1-5%	5%
Background normalization error	2-10%	10%
For $\nu$ NC disappearance studies		
$\nu$ NC efficiency	70-95%	90%
$\nu_\mu$ CC mis-identification rate	2-10%	10% *
$\nu_e$ CC mis-identification rate	1-10%	10% *
Other background	0%	0%
Signal normalization error	1-5%	
Background normalization error	2-10%	
Neutrino energy resolutions		
$\nu_e$ CC energy resolution	$15\%/\sqrt{E(\text{GeV})}$	$15\%/\sqrt{E(\text{GeV})}$
$\nu_\mu$ CC energy resolution	$20\%/\sqrt{E(\text{GeV})}$	$20\%/\sqrt{E(\text{GeV})}$
$E_{\nu_e}$ scale uncertainty		
$E_{\nu_\mu}$ scale uncertainty	1-5%	2%

[LABEL: "tab:lar-nuosc-totaltable"]

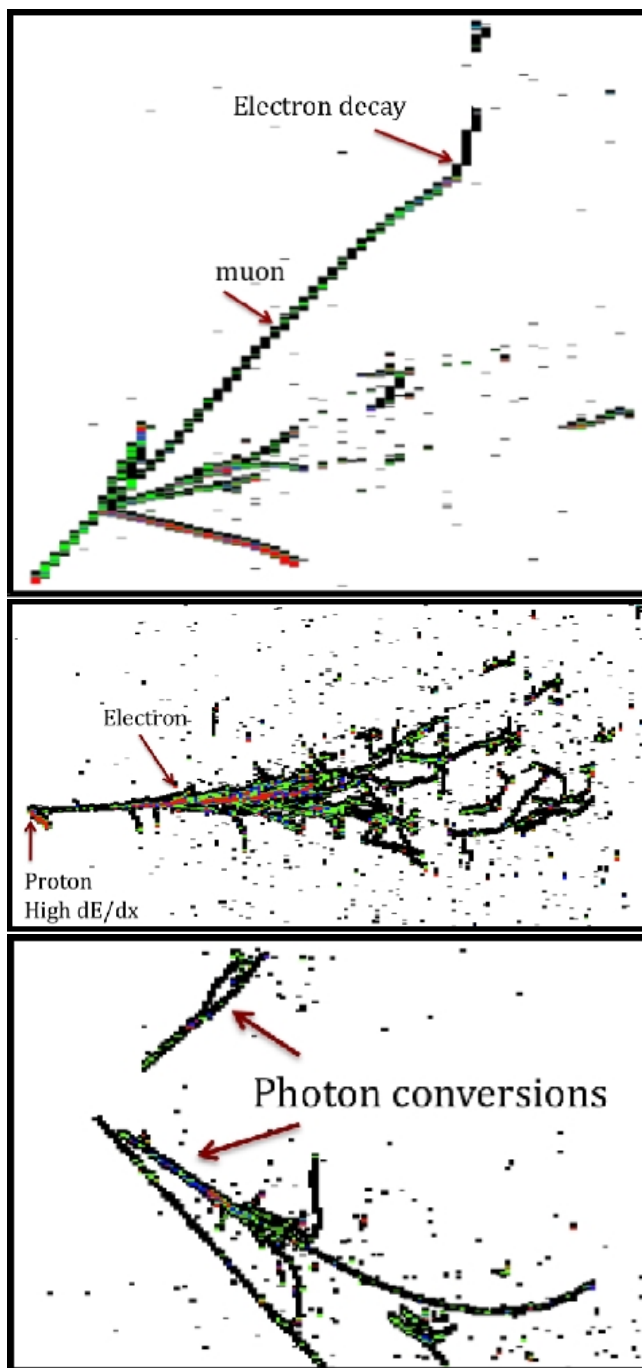


**Figure 6-3:** Examples of neutrino beam interactions in an LArTPC obtained from the Fermilab study of 2008. **FIXME:** add reference A CC  $\nu_\mu$  interaction with a stopped  $\mu$  followed by a decay Michel electron (top), a QE  $\nu_e$  interaction with a single electron and a proton (middle), an NC interaction which produced a  $\pi^0$  that then decayed into two  $\gamma$ 's with separate conversion vertices (bottom)

[LABEL: "fig:lar-scan-events"]

**Table 6–3:** Description of the LAr-TPC simulations used to determine the performance for beam neutrino interactions.

Study	TPC geometry	Analysis technique
T2K 2km proposal [12] (2005)	140 tons, 4.5m(w)x4.5m(h)x5m(l) 2 readout chambers, 2 planes/chamber 3mm/6.4m wire pitch/length 2.21m/1.1ms max drift distance/time	Fully automated reconstruction, event topology, $\mu/\pi^\pm/K/p^+$ dE/dX and event kinematics included in a Random Forest analysis
Tufts Visual Scan [13] (2006)	Unknown	Blind visual scan visible energy precuts topology only
FNAL Visual Scan [14] (2008)	2.5m(w)x2.5m(h)x2.5m(l) 1 readout chamber, 2 planes/chamber 5mm and 10mm wire pitch	Blind visual scan MC truth used in precuts topology and dE/dX included in a log-likelihood analysis
FNAL Visual Scan [15] (2011)	MicroBooNE TPC	Blind visual scan topology only

[LABEL: “tab:lar-perf-studies”]

[12]. The simulated geometry of the TPC for the 2km T2K proposal is summarized in Table 6–3. This study is the only one to use fully automated 3-D event reconstruction combined with dE/dX particle id and event kinematics in an automated analysis. The neutrino event reconstruction and analysis were optimized to separate  $\nu_\mu$  CC and  $\nu_\mu$  NC separation, but did not include  $e/\pi^0$  separation. As a result, the observed rate of 6.9% of NC events mis-identified as  $\nu_e$  CC is an over-estimate. A separate likelihood analysis of single electrons and  $\pi^0$  interactions in the T2K 2km LAr-TPC demonstrated that the single  $\pi^0$  mis-id rate can be reduced to few % using dE/dX alone as shown in Figure 6–4. Therefore, the 6.9% NC mis-identification rate could be greatly reduced by including  $e/\pi^0$  separation in the analysis.

The last 3 studies in Table 6–3 comprise visual scans of simulated events in which researchers are trained to identify  $\nu_e$ ,  $\nu_\mu$  and NC  $\pi^0$  interactions by studying event displays on an event-by-event basis. After training, the scanners are presented with a mixed sample of simulated events and asked to categorize them. Efficiencies are determined by comparing the scanners’ results to the known event type. The selection efficiencies for signal neutrino interactions and rejection efficiencies for NC background, determined by the four studies summarized here are shown in Table 6–4. There is a general agreement between all 4 studies that the efficiency for identifying  $\nu_e$  CC events in the few GeV range is in the range of 70 to 95%. In addition, we find that the reconstruction efficiency of  $\nu_e$  CC as a function of neutrino energies is approximately flat for neutrino energies  $> 1$  GeV as shown in Figure 6–5. The mis-identification rate of  $\nu_\mu$  CC events obtained from these studies is around 2%. Since optimized  $e/\mu$  separation using dE/dX has not yet been implemented in these studies, the

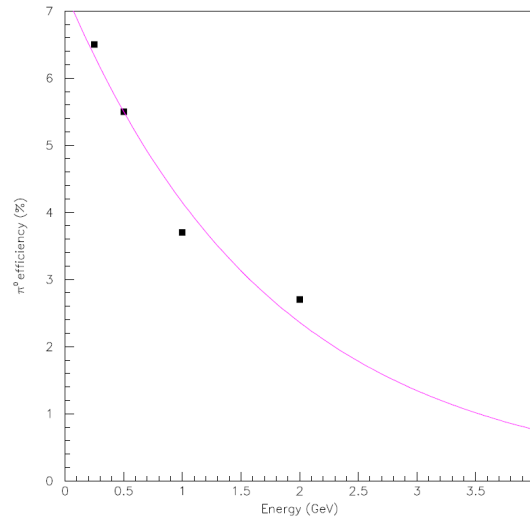


**Figure 6-4:** The electron mis-identification rate of single  $\pi^0$  interactions as a function of the incoming  $\pi^0$  energy [12].

**[LABEL: “fig:lar-perf-pi0misid”]**

1 2%  $\nu_\mu$  mis-identification rate will be considered an upper limit. There is a large variation  
 2 observed in the NC mis-identification rate. The lowest NC mis-id rate was obtained by the  
 3 visual scan study that included a crude  $dE/dX$  measurement combined with topology [14].  
 4 The estimation of the NC mis-identification rate is further complicated by the fact that  
 5 only the last study in Table 6-4 simulated  $\nu$  NC interactions with energies  $> 5$  GeV. In  
 6 the search for  $\nu_e$  appearance by the MINOS experiment [16] - which has a beam neutrino  
 7 spectrum and  $\nu_e$  signal range very similar to LBNE - it was observed that  $\approx 50\%$  of the  
 8 NC background in the 1-5 GeV signal region originated from NC inelastic interactions with  
 9 neutrino energies  $> 5$  GeV. An example of the complicated topology of deep inelastic NC  
 10 interactions is shown in Figure 6-6. We do not yet have reliable estimates of the NC mis-  
 11 identification rate of such events. Given the current knowledge of LAr-TPC performance from  
 12 these studies, we estimate that the LBNE NC mis-identification is between 2% (conservative)  
 13 to 0.4% (aggressive) depending on how well  $e/\pi^0$  separation techniques will perform in more  
 14 complicated topologies.

15 For the neutrino-oscillation sensitivity calculations, information from these hand scans are  
 16 used to set the detector signal efficiencies and background-rejection efficiencies. Table 6-2  
 17 shows the range of  $\nu_e$  selection efficiencies, background levels, and neutrino energy resolutions  
 18 from the hand scans in Table 6-4, along with the specific values chosen for the long-baseline  
 19 oscillation-sensitivity projections.

20 Studies from ICARUS have estimated and measured single-particle energy resolutions in  
 21 liquid argon. Below 50 MeV, the energy resolution of electrons is  $11\%/\sqrt{E[MeV]} + 2\%$ .  
 22 As shown in Figure 6-7, the energy resolution of an electromagnetic shower with energy in  
 23 the range (50-5000) MeV is  $33\%/\sqrt{E(MeV)} + 1\%$  [1]. The energy resolution of hadronic

**Table 6-4:** Selection efficiencies for  $\nu_e$  CC candidates and  $\nu_e$  mis-identification rates for  $\nu_\mu$  CC and  $\nu_\mu$  NC determined by various studies. The / symbol indicates samples where the event size was too small to draw meaningful conclusions.

Study	Average $\nu$ energy	# events studied	$\nu_e$ CC $\epsilon_{\text{select}}$	$\nu_\mu$ CC $\epsilon_{\text{mis-id}}$	$\nu_\mu$ NC $\epsilon_{\text{mis-id}}$
T2K 2km proposal (2005)	0.25-4.0 GeV	2000	94.5%	2%	6.9%
Tufts Visual Scan (2006)	NO $\nu$ A beam 1.5-4.5 GeV	450	$72 \pm 5\%$	/	$1.3 \pm 0.4\%$
FNAL Visual Scan (2008)	NO $\nu$ A beam 0.5-3.5 GeV	4997	$92 \pm 9\%$	/	$0.6 \pm 0.1\%$
FNAL Visual Scan (2011)	Uniform 0.5-15 GeV	1501	$90 \pm 1\%$	$2.0 \pm 0.6\%$	$5 \pm 1\%$

[LABEL: "tab:handscanresults"]

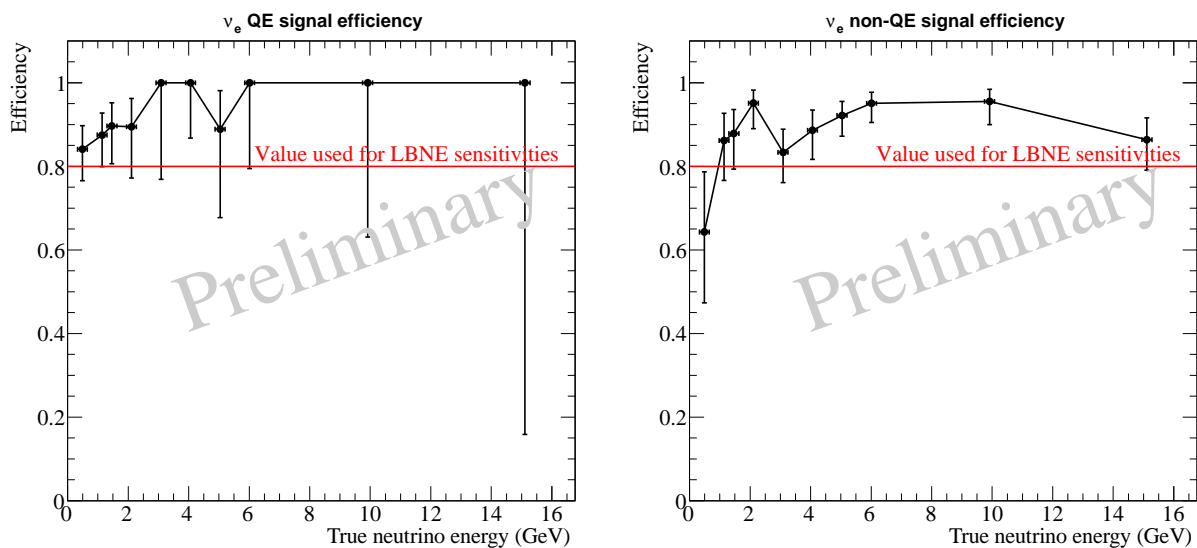


**Figure 6-5:** The efficiency, as determined by the 2011 Fermilab hand scan study [15], of selecting  $\nu_e$  CC quasi-elastic (left) and non-quasi-elastic (right) events.

[LABEL: "fig:lar-qe-nqe-eff"]

- 1 showers in a LAr-TPC is  $\approx 30\%/\sqrt{E(\text{GeV})}$  **FIXME: REF?** A significant fraction of the  $\nu_e$
- 2 CC signal in LBNE in the range of 1-6 GeV is non-quasi-elastic CC interactions with a large
- 3 component of the visible energy in the hadronic system. From recent simulations of neutrino
- 4 interactions in the region of 1-6 GeV we have determined that the  $\langle E_{\text{lepton}}/E_\nu \rangle \approx 0.6$ .
- 5 For this reason, the total electron-neutrino energy resolution for the neutrino-oscillation
- 6 sensitivity calculation is chosen to be  $15\%/\sqrt{E(\text{GeV})}$ . In a non-magnetized LAr-TPC the

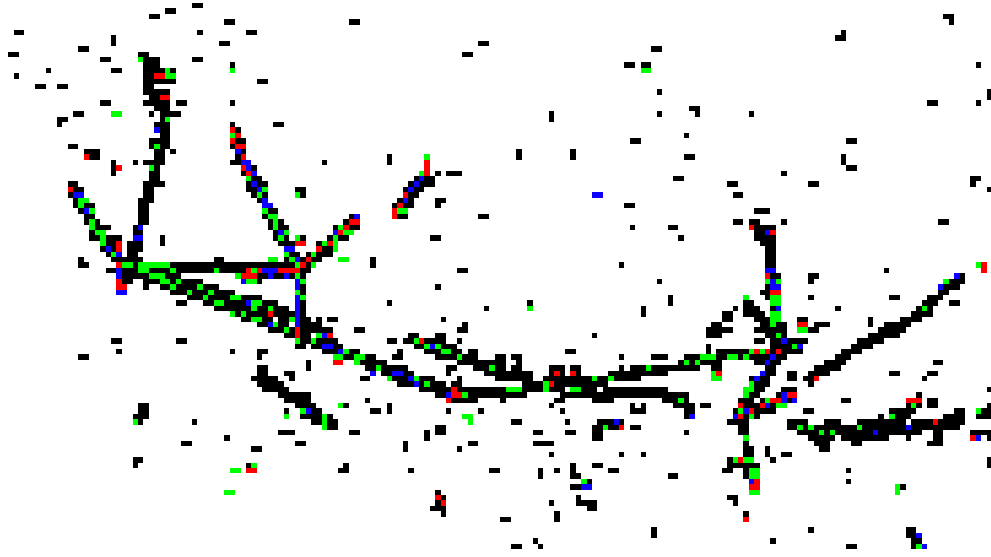


**Figure 6-6:** An example of a deep inelastic NC interaction in a LAr-TPC.  
**[LABEL: “fig:lar-event-nc-dis”]**

**Table 6-5:** Expected number of neutrino oscillation signal and background events in the energy range (0.5 - 5.0) GeV at the LAr-FD, assuming  $\sin^2(2\theta_{13}) = 0.1$  and  $\delta_{CP} = 0$ .

	Signal Events	Background Events			
	$\nu_e$	$\nu_\mu$ CC	$\nu_\mu$ NC	$\nu_e$ Beam	Total
Neutrino Normal Hierarchy	1074	66	77	92	234
Neutrino Inverted Hierarchy	477	66	77	97	240
Antineutrino Normal Hierarchy	279	29	51	46	126
Antineutrino Inverted Hierarchy	440	29	51	44	124

**[LABEL: “tab:eventcounts”]**

1 muon momentum can be obtained from range and multiple scattering and is found to be  
 2 in the range 5 – 15% [17] [12] for muons in the 1-5 GeV range **FIXME:** *Check these*  
 3 *numbers!*. Therefore the total muon-neutrino energy resolution in LBNE is assumed to be  
 4  $20\%/\sqrt{E(\text{GeV})}$ .

5 In five years of neutrino (anti-neutrino) running, assuming  $\sin^2(2\theta_{13}) = 0.1$ ,  $\delta_{CP} = 0$ , and  
 6 normal mass hierarchy, we expect 1074 (229) selected  $\nu_e(\bar{\nu}_e)$  signal events in the LAr-FD with  
 7 a 700 kW beam. Table 6-5 is a summary of the expected number of signal and background  
 8 events for  $\nu_e$  and  $\bar{\nu}_e$  running for normal and inverted hierarchy. The spectrum of expected  
 9 signal and background events is shown in Figure 6-8.

10 Figure 6-9 shows the fraction of  $\delta_{cp}$  values for which a  $3\sigma$  resolution of the mass ordering  
 11 (hierarchy) and determination of whether CP is violated ( $\delta_{cp} \neq 0$  or  $\pi$ ) is achieved by a 34 kt

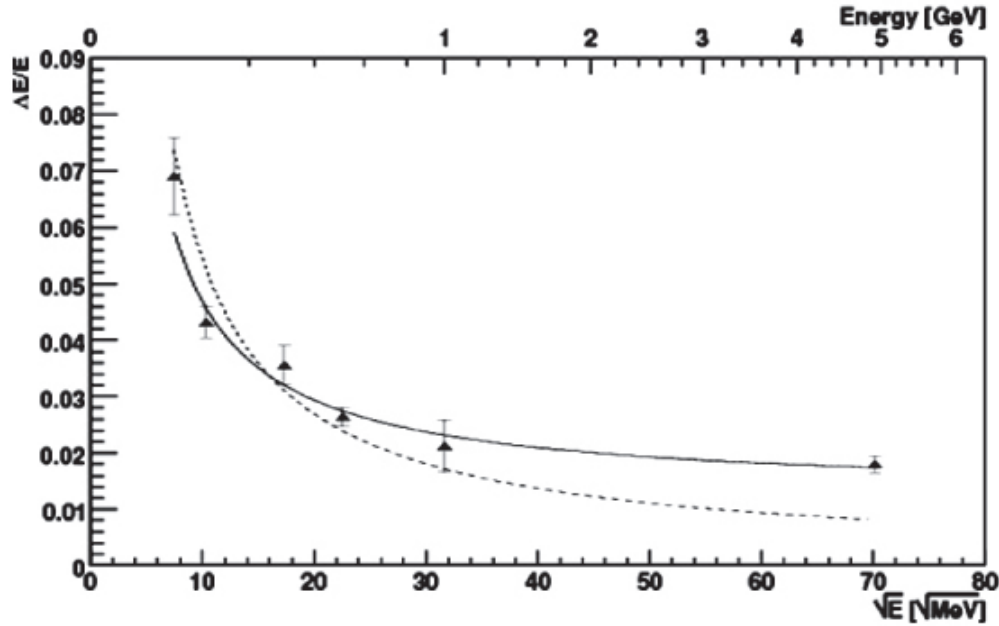


**Figure 6-7:** Resolution of electromagnetic showers from ICARUS [1]  
**[LABEL: “fig:icarusemres”]**

1 fiducial volume LAr-TPC. For values of  $\sin^2 2\theta_{13} > 0.07$ , we find that LBNE will determine  
 2 the mass hierarchy at the  $5\sigma$  level. For values of  $\sin^2 2\theta_{13} > 0.07$  LBNE will determine  
 3 whether CP is violated for 65% and 40% of all  $\delta_{cp}$  values at the 3 and 5  $\sigma$  levels respectively.  
 4 The precision on the measurements of  $\sin^2 2\theta_{13}$  and  $\delta_{cp}$  that can be achieved is shown in  
 5 Figure 6-10. LBNE will be able to measure  $\delta_{cp}$  with a precision of better than  $20^\circ$  and  
 6  $\sin^2 2\theta_{13}$  to better than 0.5%.

## 7 6.2.2 Precision Measurements of the Oscillation Parameters in $\nu_\mu \rightarrow \nu_x$ Oscillations.

8 In addition to measurements of  $\nu_e$  appearance, LBNE will make precise measurements of  
 9  $\theta_{23}$  and  $|\Delta m_{32}^2|$  using the  $\nu_\mu/\bar{\nu}_\mu$ -disappearance channel. Differences in the measured values  
 10 of  $|\Delta m_{32}^2|$  and  $|\Delta \bar{m}_{32}^2|$  are sensitive to new physics arising from NC-like non-standard inter-  
 11 actions [18] as described in Section 6.2.5.

12 The expected range of detector performance parameters for the  $\nu_\mu$ -disappearance channel  
 13 are summarized in Table 6-2. The predicted spectrum of oscillated  $\nu_\mu$  and  $\bar{\nu}_\mu$  CC events in  
 14 LBNE is shown in Figure 6-11.

15 In Figure 6-12, the result from fits of the expected spectrum of  $\nu_\mu/\bar{\nu}_\mu$  CC in the LBNE LAr-

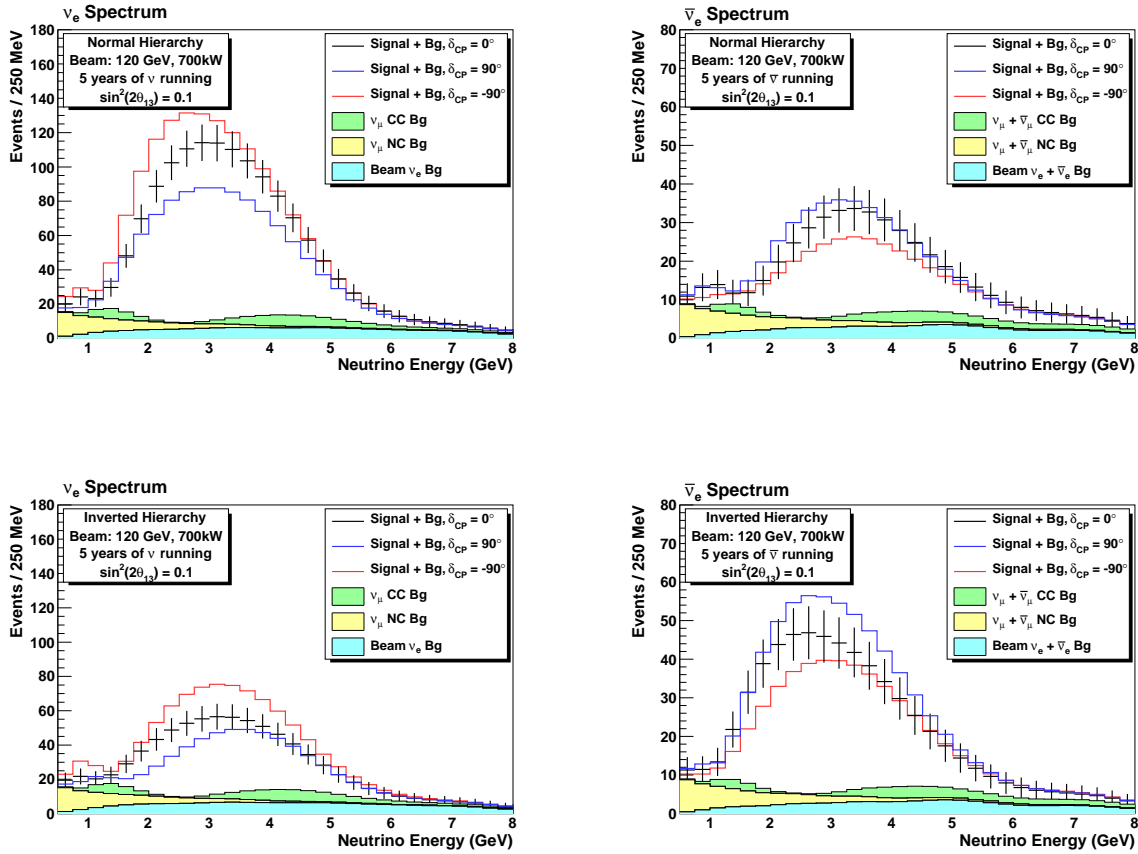


**Figure 6–8:** The expected spectrum of  $\nu_e$  or  $\bar{\nu}_e$  oscillation events in a 34 kT LArTPC for 5 years of neutrino (left) and antineutrino (right) running with a 700 kW beam, assuming  $\sin^2(2\theta_{13}) = 0.1$  for normal hierarchy (top) and inverted hierarchy (bottom). Backgrounds are displayed as stacked histograms.

[LABEL: “fig:lar-event-spectrum”]

1 FD is shown for different values of  $\Delta m_{32}^2$  and  $\sin^2 2\theta_{23}$  for neutrinos and anti-neutrinos. A  
 2  $\nu_\mu/\bar{\nu}_\mu$  CC reconstruction efficiency of 85% and a NC contamination rate of 0.5% is assumed  
 3 for these measurements. The variation on the precision of the parameters for different values  
 4 of the NC contamination is shown in Figure 6–13. The LAr-FD can achieve <1% precision  
 5 on these parameters.

### 6.2.3 Observation of $\nu_\tau$ Appearance

7 The LBNE baseline at 1300 km will be longer than any long baseline experiment currently  
 8 in operation. As a result,  $\nu_\mu$  oscillations occur at higher energy and in particular the energy  
 9 range is favorable to  $\nu_\mu \rightarrow \nu_\tau$  appearance above the  $\tau$  CC production threshold of 3.2 GeV

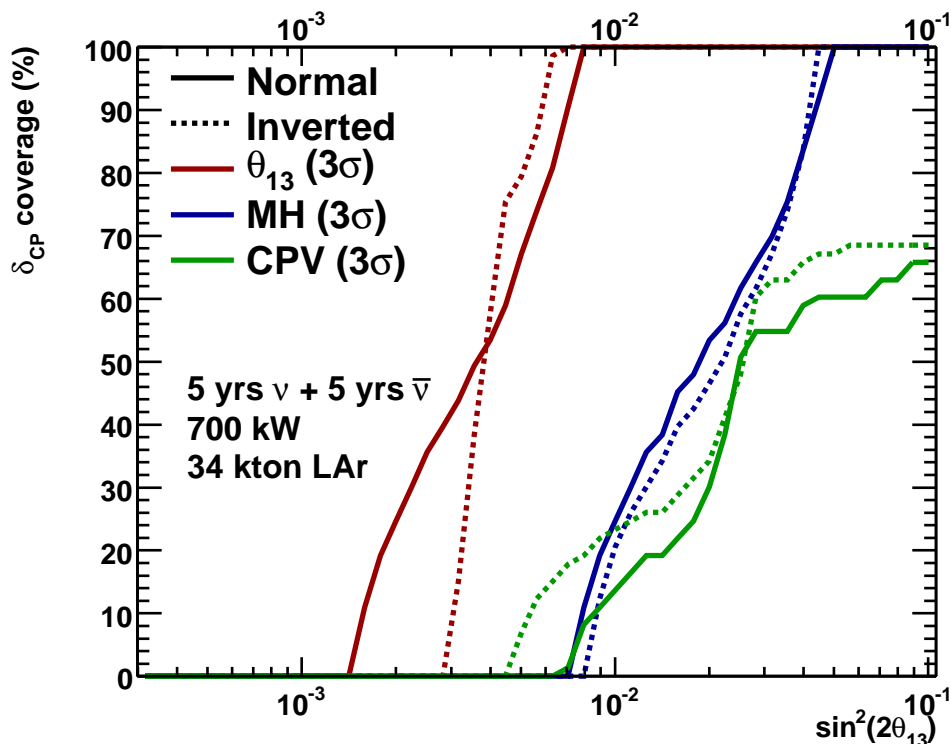


**Figure 6–9:** The fraction of  $\delta_{cp}$  values for which a  $3\sigma$  resolution of the mass ordering (hierarchy) and determination of whether CP is violated ( $\delta_{cp} \neq 0$  or  $\pi$ ) can be achieved by a 34 kt fiducial volume LArTPC for 5+5 yrs ( $\nu + \bar{\nu}$ ) running in a 700kW beam.

[LABEL: "fig:lar-cp-frac"]

1 as shown in Figure 6–14. In this respect LBNE has a unique ability compared to current  
 2 long baseline experiments in that oscillation between all three flavors of neutrinos could be  
 3 explicitly observed in a single experiment. To increase the  $\nu_\tau$  CC appearance signal, we are  
 4 considering several high energy beam tunes produced by moving the target further upstream  
 5 of an updated design of LBNE horn 1.

6 In Table 6–1,  $\nu_\tau$  CC appearance rates for several LBNE beam tunes are shown. The first  
 7 row in Table 6–1 corresponds to the baseline low-energy beam tune used for the primary  
 8 oscillation physics. The last two rows correspond to two proposed high energy beam tunes  
 9 produced by pulling the target back by 1.5 m and 2.5 m from a double parabolic horn 1.  
 10 The higher energy beam tunes can be used to greatly enhance the  $\nu_\tau$  appearance rate. In  
 11 particular, the medium-energy (ME) tune has both high  $\nu_e$  and  $\nu_\tau$  appearance rate. It is  
 12 to be noted that the OPERA-tau experiment which has seen one  $\nu_\tau$  CC interaction [19]  
 13 expects a rate of 2  $\nu_\tau$  events/1.25 kt/year compared to LBNE which would record a rate of  
 14 150  $\nu_\tau$  events/34 kt/year in the ME beam.

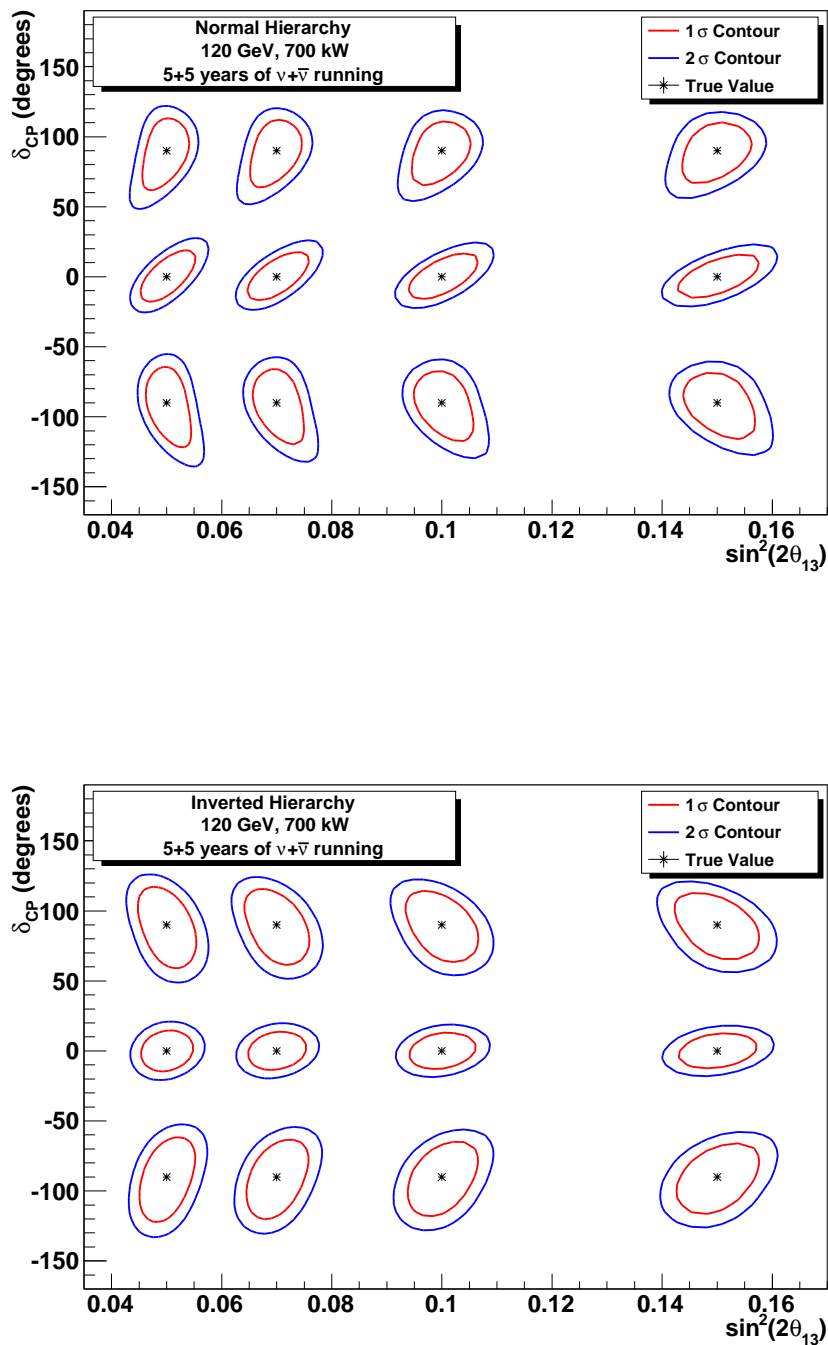


**Figure 6–10:** Fits to the values of  $\sin^2 2\theta_{13}$  and  $\delta_{cp}$  as a function of  $\sin^2 2\theta_{13}$  for normal (top) and inverted (bottom) hierarchy.

[LABEL: “fig:lar-jelly-bean”]

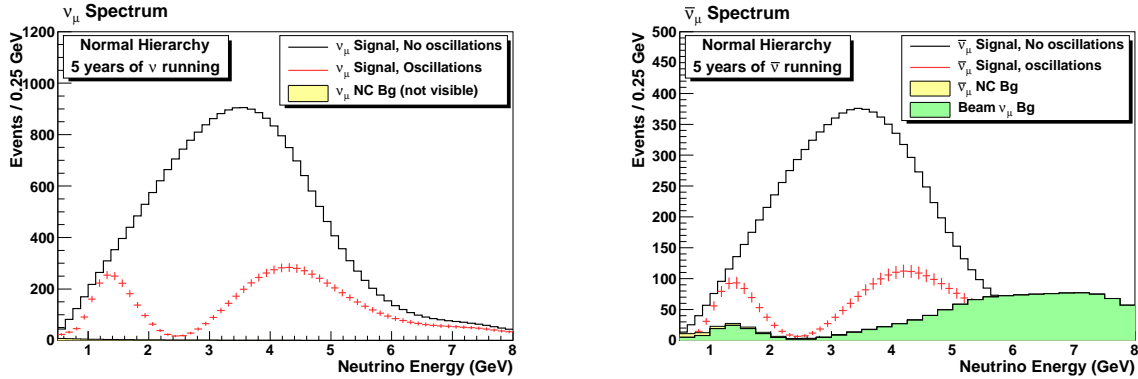


**Figure 6–11:** The expected spectrum of  $\nu_\mu$  or  $\bar{\nu}_\mu$  events in a 34 kT LArTPC for 5 years of neutrino (left) and antineutrino (right) running with a 700 kW beam, with and without neutrino oscillation.

[LABEL: “fig:lar-disapp-spectrum”]

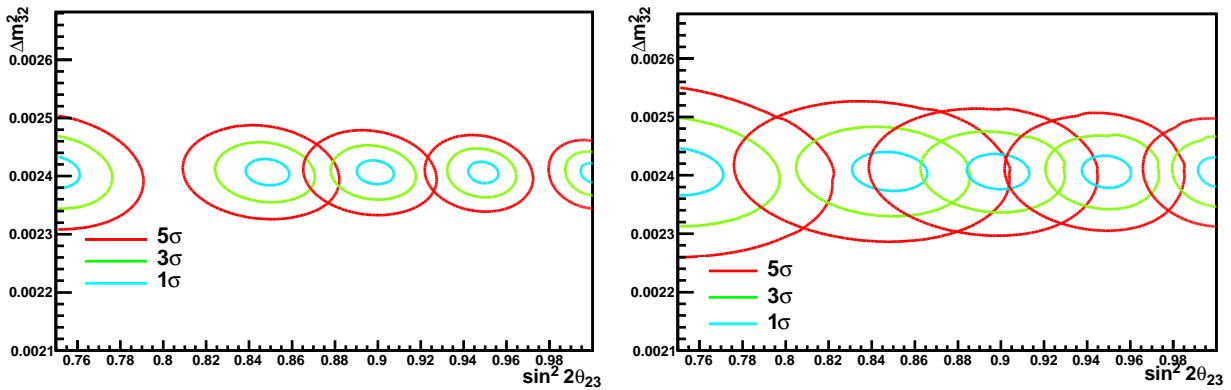


**Figure 6–12:** Fit to different values of  $\Delta m_{32}^2$  and  $\sin^2 2\theta_{23}$ , for neutrino running (left) and anti-neutrino running (right).

[LABEL: “fig:lar-disapp-fit”]

### 1 6.2.4 Resolving the $\theta_{23}$ octant

2 Current experimental results tell us that  $\sin^2 2\theta_{23}$  is near maximal ( $\sin^2 \theta_{23} > 0.91$  at 90%  
3 CL [20]), however there exist two solutions of  $\theta_{23}$  for a given set of measured oscillation  
4 parameters, known as the  $\theta_{23}$  octant ambiguity. If the oscillation associated with  $\nu_\mu$  disap-  
5 pearance is not maximal, then it will be important to determine whether  $\theta_{23}$  is greater than  
6 or less than  $\pi/4$ . This in turn will help tell us whether the third neutrino mass eigenstate  
7 couples more strongly to  $\nu_\mu$  or  $\nu_\tau$ . The value of  $\theta_{23}$  varies the  $\nu_\mu \rightarrow \nu_e$  appearance spectrum  
8 as shown in Figure 6–15. The impact of the  $\theta_{23}$  octant in the energy regions around the 2<sup>nd</sup>  
9 oscillation maximum is very small compared to the effect of  $\delta_{cp}$  - which is much larger at

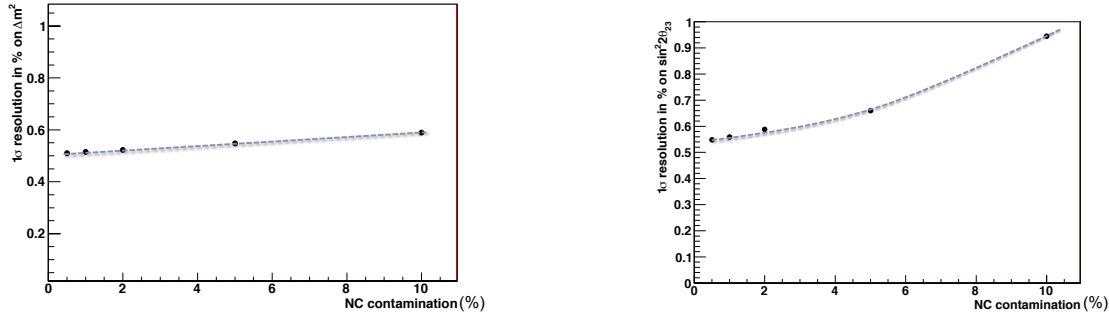


**Figure 6–13:** Impact of varying the NC contamination on the precision of measuring  $\Delta m_{32}^2$  (left) and  $\sin^2 2\theta_{23}$  (right).

[LABEL: “fig:lar-disapp-eff-nc”]

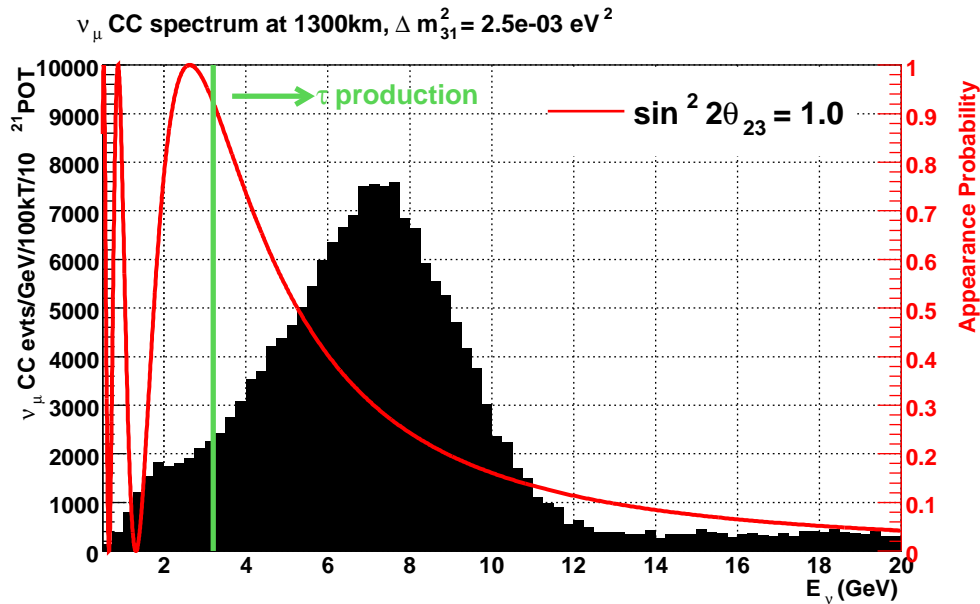


**Figure 6–14:** The  $\nu_\mu \rightarrow \nu_\tau$  oscillation probability (red curve) at 1300km for  $\sin^2 2\theta_{23} = 1.0$ . The shaded histogram is the unoscillated  $\nu_\mu$  CC spectrum at 1300km from the medium-energy (ME) beam tune.

[LABEL: “fig:nutau\_appear”]

- 1 lower energies - and is the same for neutrinos and anti-neutrinos which helps to resolve the
- 2 degeneracy with the mass hierarchy and  $\delta_{CP}$  in the region of the 1<sup>st</sup> oscillation maximum.
- 3 Figure 6–16 displays the capability of LBNE to resolve the  $\theta_{23}$  octant with the 34 kt LAr-FD.
- 4 Running in a 700 kW beam, LBNE is able to resolve the  $\theta_{23}$  octant degeneracy for  $\theta_{23}$  values
- 5 less than  $40^\circ$  at 90% CL and 90% of  $\delta_{CP}$  values if  $\sin^2 2\theta_{13}$  is greater than 0.075 for 34 kt
- 6 LAr. Improvements in the resolving power of LBNE could be achieved with more neutrino
- 7 flux at lower energies to break degeneracies with  $\delta_{CP}$  values.

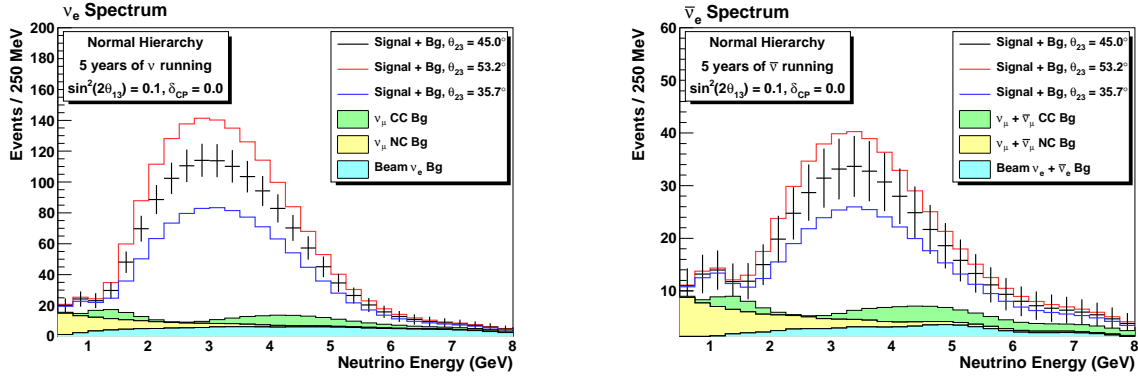


**Figure 6–15:** The expected spectrum of  $\nu_e$  or  $\bar{\nu}_e$  oscillation events in a 34 kT LArTPC for 5 years of neutrino (left) and antineutrino (right) running with a 700 kW beam, assuming normal hierarchy,  $\sin^2(2\theta_{13}) = 0.1$ ,  $\delta_{CP} = 0$  and varying the value of  $\theta_{23}$  within the current range of allowed values. Backgrounds are displayed as stacked histograms.

[LABEL: “fig:lar-event-spectrum-th23”]

## 1 6.2.5 Searches for New physics in Long Baseline Oscillations

2 [LABEL: “sec:new\_physics”]

3

4 In addition to precision measurements of the standard three-flavor neutrino oscillation pa-  
 5 rameters, LBNE is also well-suited for new physics searches in the neutrino sector. For  
 6 example, the experiment is sensitive to non-standard neutrino interactions and active-sterile  
 7 neutrino mixing, provided that these effects are not too weak.

### 8 6.2.5.1 Non-standard Interactions

9 NC non-standard interactions (NSI) can be understood as non-standard matter effects that  
 10 are visible only in a far detector at a sufficiently long baseline. This is where LBNE has a  
 11 unique advantage compared to other long-baseline experiments (except atmospheric neutrino  
 12 experiments, which are, however, limited by systematic effects). NC NSI can be parameter-  
 13 ized as new contributions to the MSW matrix in the neutrino propagation Hamiltonian:

$$H = U \begin{pmatrix} 0 & & \\ & \Delta m_{21}^2/2E & \\ & & \Delta m_{31}^2/2E \end{pmatrix} U^\dagger + \tilde{V}_{\text{MSW}}, \quad (6.1)$$

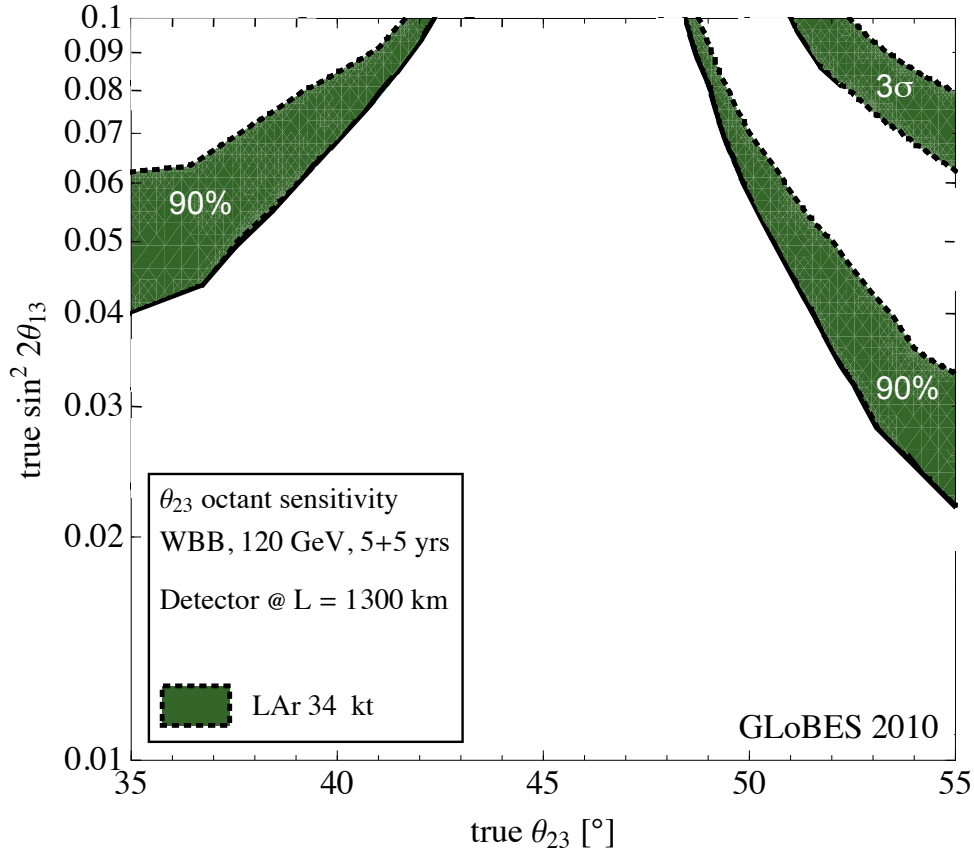


**Figure 6–16:** Sensitivity of LBNE to resolve the  $\theta_{23}$  octant degeneracy for 5+5 years of  $\nu+\bar{\nu}$  running at 700 kW and normal mass hierarchy. The green band shows the results for 34 kt LAr. The width of the bands corresponds to the impact of different true values for  $\delta_{CP}$ , ranging from a 10% to 90% fraction of  $\delta_{CP}$ . In the region above the bands, the determination of the  $\theta_{23}$  octant is possible at 90% CL (lower bands) and  $3\sigma$  (upper bands).

[LABEL: “fig:lbnl\_theta23\_octant”]

with

$$\tilde{V}_{\text{MSW}} = \sqrt{2}G_F N_e \begin{pmatrix} 1 + \epsilon_{ee}^m & \epsilon_{e\mu}^m & \epsilon_{e\tau}^m \\ \epsilon_{e\mu}^{m*} & \epsilon_{\mu\mu}^m & \epsilon_{\mu\tau}^m \\ \epsilon_{e\tau}^{m*} & \epsilon_{\mu\tau}^{m*} & \epsilon_{\tau\tau}^m \end{pmatrix} \quad (6.2)$$

<sup>1</sup> Here,  $U$  is the leptonic mixing matrix, and the  $\epsilon$ -parameters give the magnitude of the NSI  
<sup>2</sup> relative to standard weak interactions. For new physics scales of few  $\times 100$  GeV, we expect  
<sup>3</sup>  $|\epsilon| \lesssim 0.01$ .

<sup>4</sup> To assess the sensitivity of LBNE to NC NSI, we define the NSI discovery reach in the  
<sup>5</sup> following way: We simulate the expected event spectra, assuming given “true” values for the  
<sup>6</sup> NSI parameters, and then attempt a fit assuming no NSI. If the fit is incompatible with the  
<sup>7</sup> simulated data at a given confidence level, we say that the chosen “true” values of the NSI

1 parameters are within the experimental discovery reach. In Figure 6-17, we show the NSI  
2 discovery reach of LBNE for the case where only one of the  $\epsilon_{\alpha\beta}^m$  parameters is non-negligible  
3 at a time [21].

4 We conclude from the figure that LBNE will be able to improve model-independent bounds  
5 on NSI in the  $e$ - $\mu$  sector by a factor of 2, and in the  $e$ - $\tau$  sectors by an order of magnitude.

### 6 6.2.5.2 Long Range Interactions

7 The small scale of neutrino mass differences implies that minute differences in the inter-  
8 actions of neutrinos and anti-neutrinos with background sources can be detected through  
9 perturbations to the time evolution of the flavor eigenstates. The longer the experimental  
10 baseline, the more sensitivity to a new long-distance potential acting on neutrinos. For ex-  
11 ample some of the models for such long-range interactions (LRI) as described in [?] could  
12 contain discrete symmetries that stabilize the proton and a dark matter particle and thus  
13 provide new connections between neutrino, proton decay and dark matter experiments. The  
14 longer baseline of LBNE coupled with the expected precision of better than 1% on the  $\nu_\mu$   
15 and  $\bar{\nu}_\mu$  oscillation parameters improves the sensitivity to LRI beyond that possible by the  
16 current generation of long baseline neutrino experiments.

### 17 6.2.5.3 Search for Active Sterile Neutrino Mixing

18 Searches for evidence of active sterile neutrino mixing at LBNE can be conducted by exam-  
19 ining the NC event rate at the far detector and comparing it to a precision measurement of  
20 the expected rate from the near detector. Observed deficits in the NC rate could be evidence  
21 for active sterile neutrino mixing. The latest such search in a long baseline experiment was  
22 conducted by the MINOS experiment [Phys.Rev.D81:052004,2010]. The expected rate of NC  
23 interactions with visible energy  $> 0.5$  GeV in LBNE is approximately 5K events over 5 yrs  
24 (see Table 6-1). The NC identification efficiency is high with a low rate of  $\nu_\mu$  CC background  
25 mis-identification as shown in Table 6-2. The LBNE will provide a unique opportunity to  
26 revisit this search with higher precision over a large range of neutrino energies.

## 27 6.3 Searches for Baryon Number Non-Conservation

28 Proton decay, and similar processes such as nucleon-antinucleon oscillation, test conservation  
29 of baryon number. Non-conservation of baryon number has never been observed; while it is  
30 predicted by many grand unified theories, it is not allowed in the Standard Model. For this  
31 reason, even a single detected event would be evidence of physics beyond the Standard Model  
32 and would strongly support the idea of grand unification.

### NC NSI discovery reach (3σ C.L.)

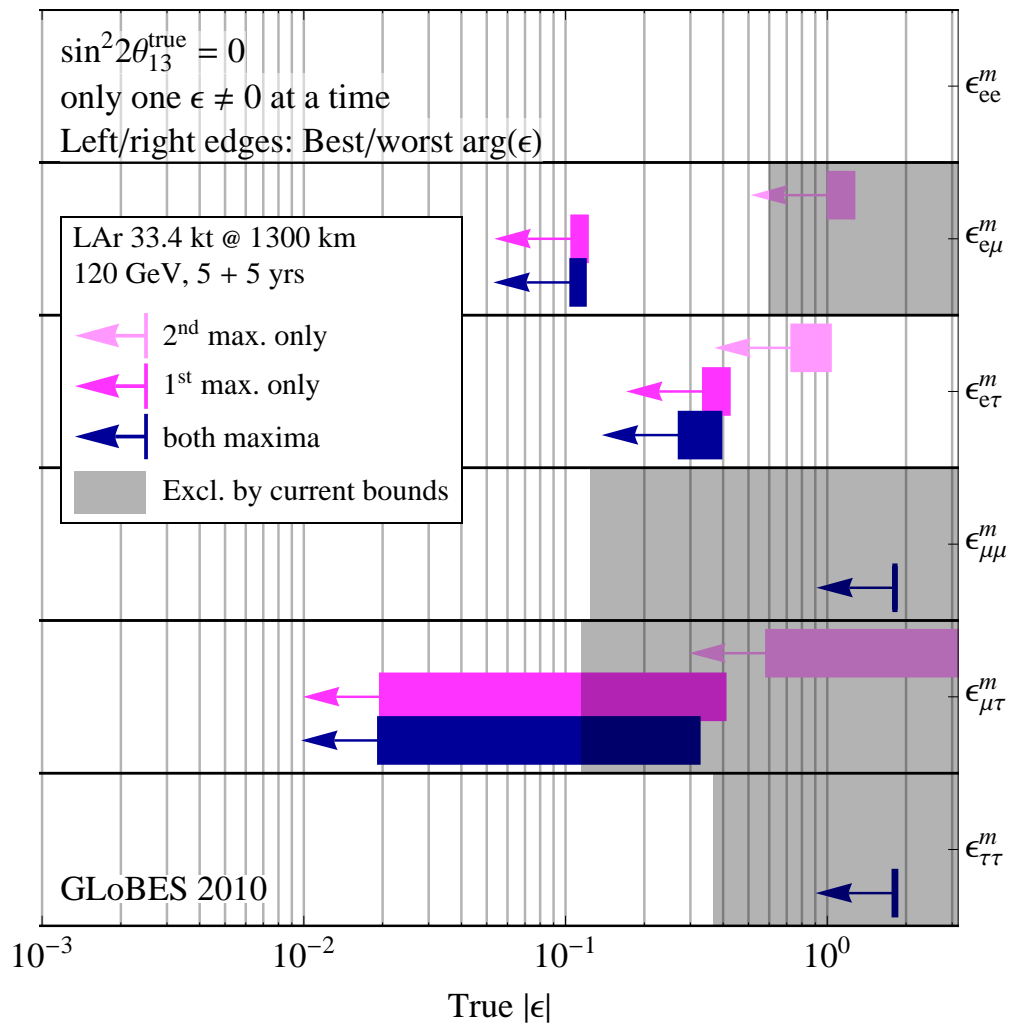


**Figure 6-17:** Non-standard interaction discovery reach in LAr-TPC. The left and right edges of the error bars correspond to the most favorable and the most unfavorable values for the complex phase of the respective NSI parameters. Red arrows indicate the current model-independent limits on the different parameters at 3 σ [22,23,24].

[LABEL: "fig:LAr-NSI"]

### 6.3.1 Proton Decay

Figure 6-18 shows experimental limits on proton decay, dominated by recent results from Super-Kamiokande, compared to the ranges of lifetimes predicted by an assortment of GUTs. From the body of literature, two decay modes emerge that dominate experimental designs. First, there is the decay mode of  $p \rightarrow e^+\pi^0$  that arises from gauge mediation. This is the most famous proton decay mode, often predicted to have the highest branching fraction, and also demonstrably the most straightforward experimental signature for a water Cherenkov detector. The total mass of the proton is converted into the electromagnetic shower energy of the positron and the two photons from  $\pi^0$  decay, with a net momentum vector near zero. The second key mode is  $p \rightarrow K^+\nu$ . This mode is dominant in most supersymmetric-GUTs, which also often favor several other modes involving kaons in the final state. This is due to the simple fact that the interaction would proceed via SUSY-Higgs exchange, which couples most strongly to quarks with the largest mass. The strange quark is the heaviest one with mass less than the nucleon mass.

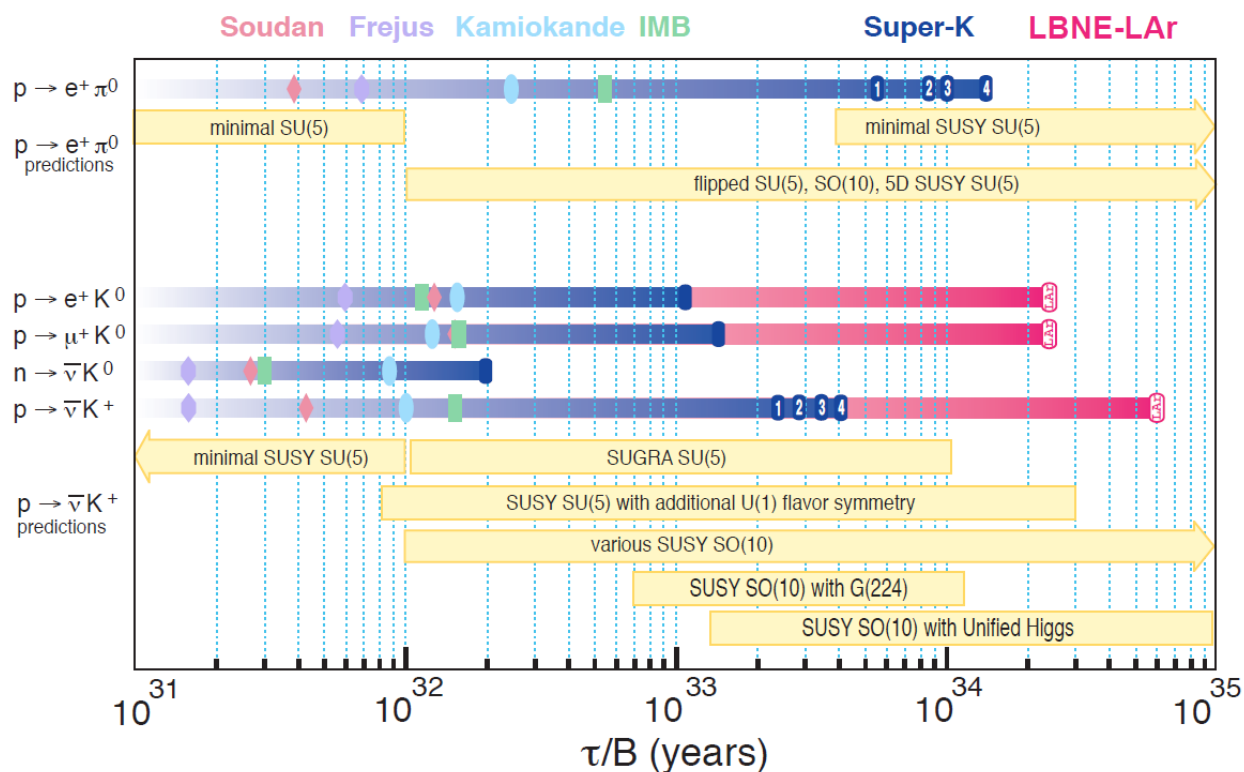


**Figure 6-18:** Proton decay lifetime limits compared to lifetime ranges predicted by Grand Unified Theories. The upper section is for  $p \rightarrow e^+\pi^0$ , most commonly caused by gauge mediation. The lower section is for SUSY motivated models, which commonly predict decay modes with kaons in the final state. The marker symbols indicate published limits by experiments, as indicated by the sequence and colors on top of the figure.

[LABEL: "PDK-limits-theory"]

- 1 The expected efficiency and background rates for the main experimental proton decay modes  
 2 are summarized in Table 6-6. For  $p \rightarrow e^+\pi^0$ , a liquid argon TPC of fiducial mass 34 kilotons  
 makes no improvement over the projected Super-K limit by itself.

Mode	Efficiency	Background Rate (evts/100 kt-y)
B-L		
$p \rightarrow e^+\pi^0$	45%	0.1
$p \rightarrow \nu K^+$	97%	0.1
$p \rightarrow \mu^+ K^0$	47%	< 0.2
B+L		
$p \rightarrow \mu^-\pi^+ K^+$	97%	0.1
$p \rightarrow e^+ K^+$	96%	< 0.2
$\Delta B = 2$		
$N\bar{N} \rightarrow n(\pi)$	TBD	TBD

**Table 6-6:** [LABEL: "tab:PDK-ffic-bg"]

Liquid argon efficiency and background numbers used for proton decay sensitivity calculations obtained from the paper by Bueno *et al.* [2].

3

- 4 LBNE has a unique sensitivity to  $p \rightarrow K^+\bar{\nu}$  because the event signature is highly described  
 5 by an LArTPC. This is because the momentum of the kaon will result in high ionization  
 6 density which can be compared to the range of the kaon. In addition, the charged kaon decays  
 7 at rest to fully reconstructible final states, so high signal efficiency with low background is  
 8 possible. Figure 6-19 shows a LArSoft [25] simulation of a  $K^+$  decay. Reference [2] finds  
 9 that an LArTPC has 97% detection efficiency for this mode, with a background rate of 0.1  
 10 events/100 kt-year.

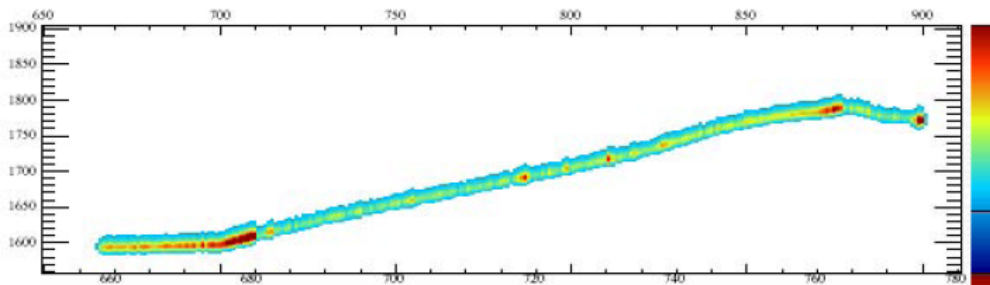


**Figure 6-19:** LArSoft simulation of  $K^+ \rightarrow \mu^+ \rightarrow e^+$  decay in the MicroBooNE geometry. The drift time is along the vertical axis. The wire number is along the horizontal axis (3-mm wire spacing).

[LABEL: "fig:kdk\_mu"]

- 11 The most serious background to  $p \rightarrow K^+\bar{\nu}$  is from cosmogenic neutral kaons undergoing  
 12 charge-exchange in the detector; in [2] this background is reduced using muon-veto detectors

1 and fiducial cuts, but for LAr-FD at the 4850L no additional background rejection is required.  
 2 Another background to  $p \rightarrow K^+\bar{\nu}$  could result from misidentified atmospheric pions. For  
 3 this reason, the ability to differentiate between kaons, pions, and muons in the LAr-FD  
 4 is important for sensitivity to proton decay. Figure 6-1 shows the particle identification  
 5 capabilities of a LAr-TPC.

6 Figure 6-20 shows the proton-decay lifetime limit as a function of time for  $p \rightarrow K^+\bar{\nu}$  for  
 7 Super-Kamiokande and LBNE. The LAr-FD can produce significant improvement to the  
 8 proton lifetime limit for  $p \rightarrow K^+\bar{\nu}$ .

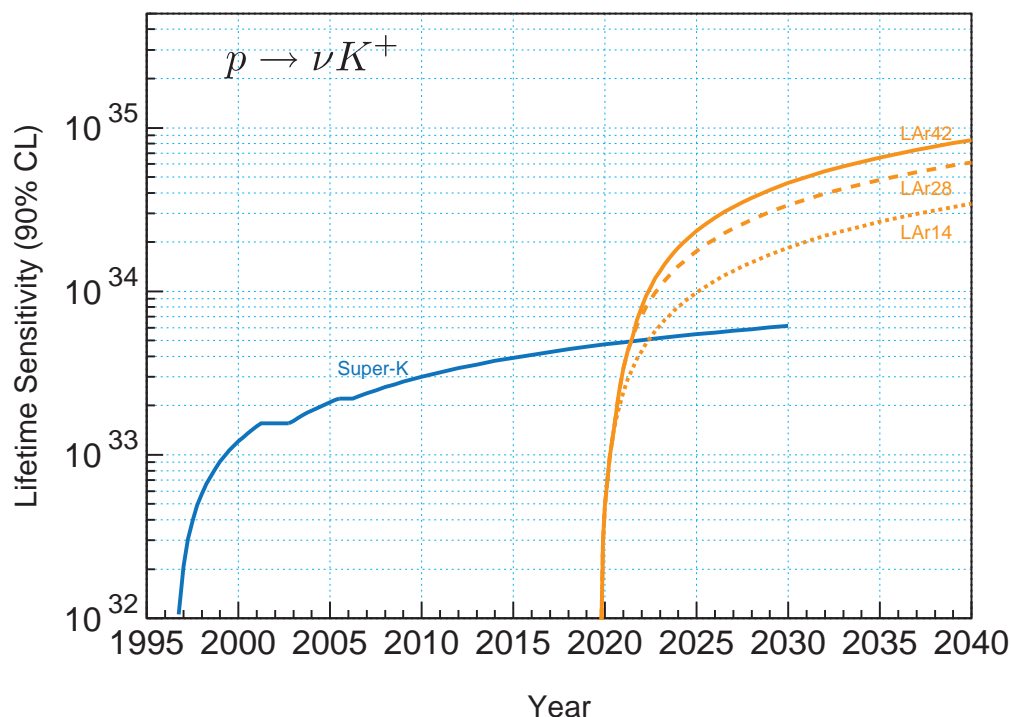


**Figure 6-20:** Proton decay lifetime limit for  $p \rightarrow K^+\bar{\nu}$  as a function of time for Super-Kamiokande compared to 14-, 28-, and 42 kt fiducial LArTPCs starting in 2019. LAr-FD at the 4850L has a fiducial mass of 34 kt. The limits are at 90% C.L., calculated for a poisson process including background assuming the detected events equals the expected background.

[LABEL: "fig:kdklimit"]

### 9 6.3.2 Nucleon/Anti-Nucleon Oscillations

10 Nucleon anti-nucleon ( $N\bar{N}$ ) oscillations will result in nearly 2 GeV of energy being released  
 11 in the detector when the oscillated anti-nucleon annihilates with a nearby nucleon, typically  
 12 producing a number of pions. Backgrounds arise mainly from atmospheric-neutrino interac-  
 13 tions that have multiple pions in the final state. An event display of a simulated event is  
 14 shown in Figure 6-21. The ability of the LAr-FD to precisely discriminate electrons from

1 photons will allow for excellent  $\pi^0$  mass and energy reconstruction in this mode and in other  
 2 nucleon-decay modes with a  $\pi^0$ . The detection efficiencies for these modes are subject to an  
 3 efficiency loss caused by nuclear effects that can absorb the pion or cause it to scatter or  
 4 charge-exchange.

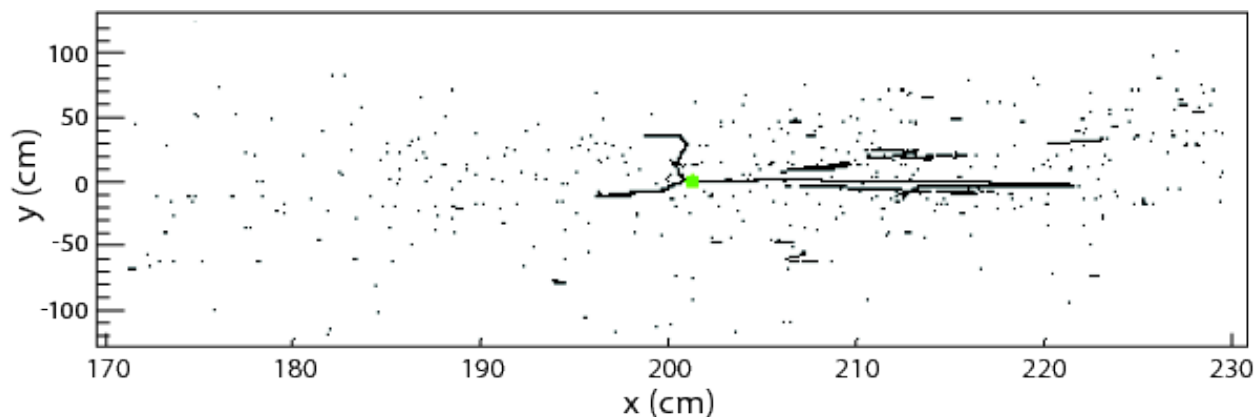


**Figure 6-21:** LArSoft simulated event,  $p\bar{p}$  annihilation at rest  
 [LABEL: “fig:PPbaranno5”]

## 5 6.4 Supernova Burst Neutrinos

6 If a core collapse supernova occurs in our galaxy during the lifetime of LBNE, the LAr-FD  
 7 will detect the associated burst of neutrinos. The explosion mechanism is thought to have  
 8 three distinct stages: the collapse of the iron core, with the formation of the shock and its  
 9 breakout through the neutrinosphere; the accretion phase, in which the shock temporarily  
 10 stalls at the radius of about 200 km, while the material keeps raining in; and the cooling  
 11 stage, in which the hot proto-neutron star loses its energy and trapped lepton number, while  
 12 the reenergized shock expands to push out the rest of the star. All these stages are predicted  
 13 to have distinct signatures in the neutrino signal. Thus, it should be possible to directly  
 14 observe, for example, how long the shock is stalled. More exotic features of the collapse may  
 15 be observable in the neutrino flux as well, such as possible transitions to quark matter or to  
 16 a black hole. (An observation in conjunction with a gravitational wave detection would be  
 17 especially interesting.)

18 Supernova neutrinos are emitted in a few tens of seconds duration, with about half in the  
 19 first second, have energies of a few tens of MeV, and have their luminosity divided roughly  
 20 equally between the three neutrino flavors. In addition to shedding light on the explosion  
 21 mechanisms of the supernova, the detection of supernova burst neutrinos would allow for a  
 22 wealth of neutrino oscillation physics measurements ranging from independent determination  
 23 of the neutrino mass hierarchy to the equation of state of matter at nuclear densities, to  
 24 constraints on physics beyond the Standard Model. Neutrinos from a core collapse arrive

1 earlier than electromagnetic radiation; the detection of a neutrino signal would provide an  
 2 alert for astronomers, allowing the observation of light-curves in early stages of the supernova.  
 3 The expected rate of core collapse supernovae in the Milky Way is 2-3 per year; in a 20 year  
 4 lifetime, there is a 40% chance for LBNE to observe such an event.

5 The sensitivity to physics associated with a supernova burst is determined by the total  
 6 detector mass. Figure 6-22 shows the neutrino event rates as function of observed energy  
 7 for a 34-kT fiducial LArTPC using the Livermore model [26] of supernova neutrino flux.  
 8 Table 6-7 lists the event rates predicted by both the Livermore model and the GKVM  
 9 model **FIXME: Add reference**. The primary sensitivity is to the  $\nu_e$  component.

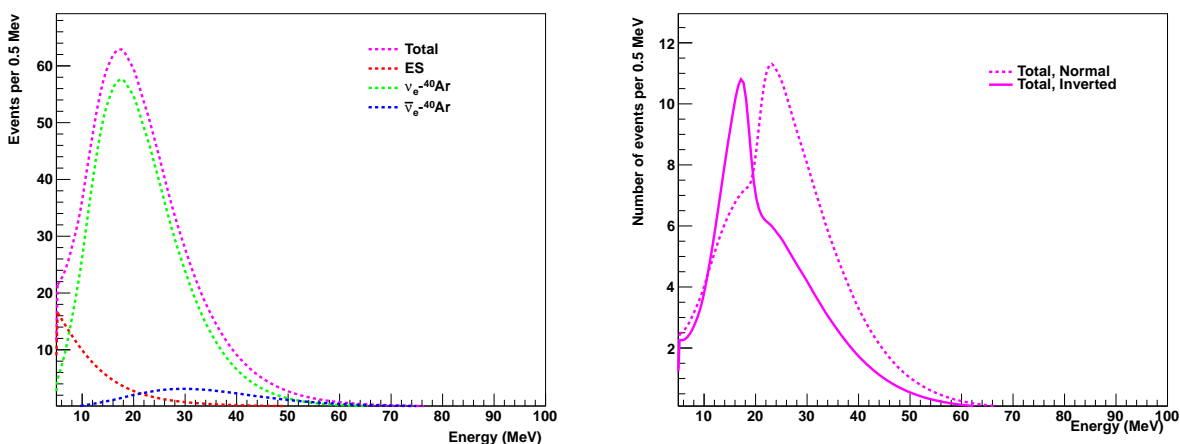


**Figure 6-22:** Event rates (per 0.5 MeV) in a 34-kt LArTPC as a function of observed energy for the Livermore model [26] of supernova neutrino flux (left), and comparison of total event rates (per 0.5 MeV) for normal and inverted hierarchies, for a late-time slice of a different flux model in a 34 kt LAr module (right).

[LABEL: “fig:SNspectra”]

Channel	Events, “Livermore” model	Events, “GKVM” model
$\nu_e + {}^{40}\text{Ar} \rightarrow e^- + {}^{40}\text{K}^*$	2308	2848
$\bar{\nu}_e + {}^{40}\text{Ar} \rightarrow e^+ + {}^{40}\text{Cl}^*$	194	134
$\nu_x + e^- \rightarrow \nu_x + e^-$	296	178
Total	2794	3160

**Table 6-7:** Supernova burst neutrino event rates for different models in 34 kt of LAr.

[LABEL: “tab:argon\_events”]

10 Figure 6-22 also compares event rates for normal and inverted hierarchies in a 34-kt LArTPC,  
 11 for a late-time slice of the  $\nu_e$  spectrum in a particular flux model. The difference between  
 12 the hierarchies is quite dramatic.

1 Initial estimates of cosmogenic backgrounds to the signal of supernova neutrinos in a LAr  
 2 detector at Homestake mine are documented in reference [?]. The location at the 4850L  
 3 will significantly reduce the background level and backgrounds in the LAr-TPC will be well-  
 4 characterized and can be statistically subtracted from the burst signal.

## 5 6.5 Atmospheric Neutrinos

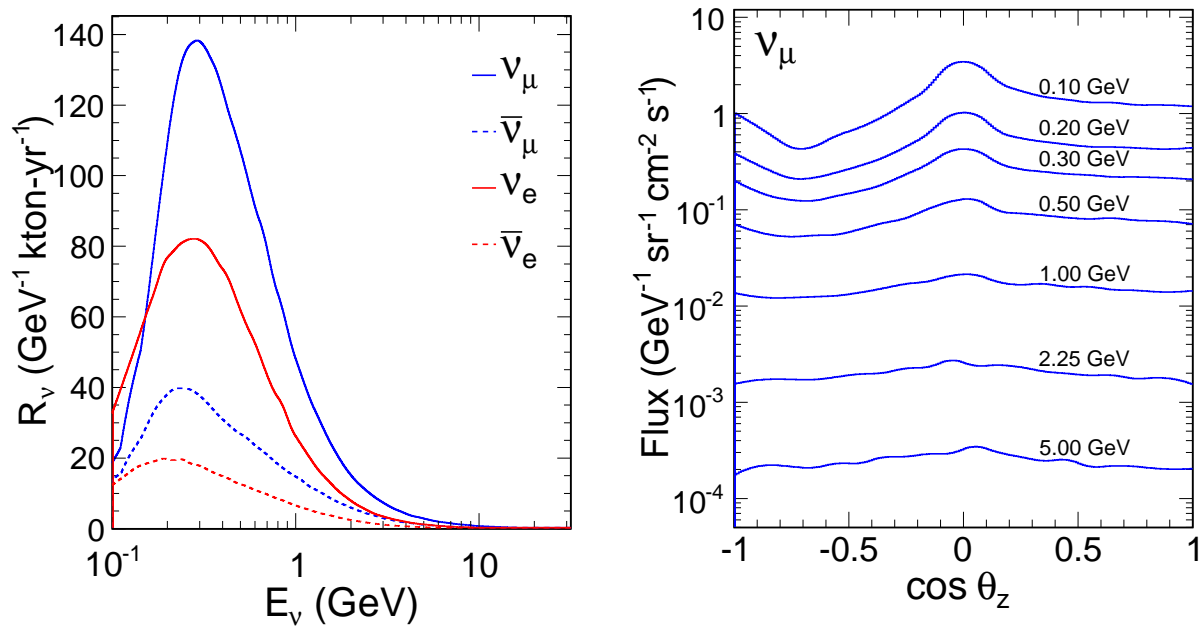


**Figure 6–23:** The expected atmospheric neutrino event rate obtained from the Bartol model at solar maximum (calculated for the Soudan mine). The energy spectrum of atmospheric neutrinos for different species is shown on the left and the angular distribution of the  $\nu_\mu$  flux is shown on the right.

[LABEL: “fig:atnu\_flux”]

6 Atmospheric neutrinos are unique among sources used to study oscillations: the oscillated  
 7 flux contains neutrinos and anti-neutrinos of all flavors, and matter effects play a significant  
 8 role. Since the oscillation phenomenology plays out over several decades in energy (see Figure  
 9 6–24) and path length, atmospheric neutrinos are very sensitive to alternative explanations or  
 10 subdominant new physics effects that predict something other than the characteristic (L/E)  
 11 dependence predicted by oscillations in the presence of matter. This power has already been  
 12 exploited by the Super-Kamiokande in fits that compare their data binned in terms of energy  
 13 and zenith angle to a host of new physics including CPT violation [27,28], Lorentz invariance  
 14 violation [29,30], non-standard interactions [31], Mass Varying Neutrinos (MaVaNs) [32], and  
 15 sterile neutrinos [33,34,35]. In numerous cases the best limits on exotic scenarios comes from

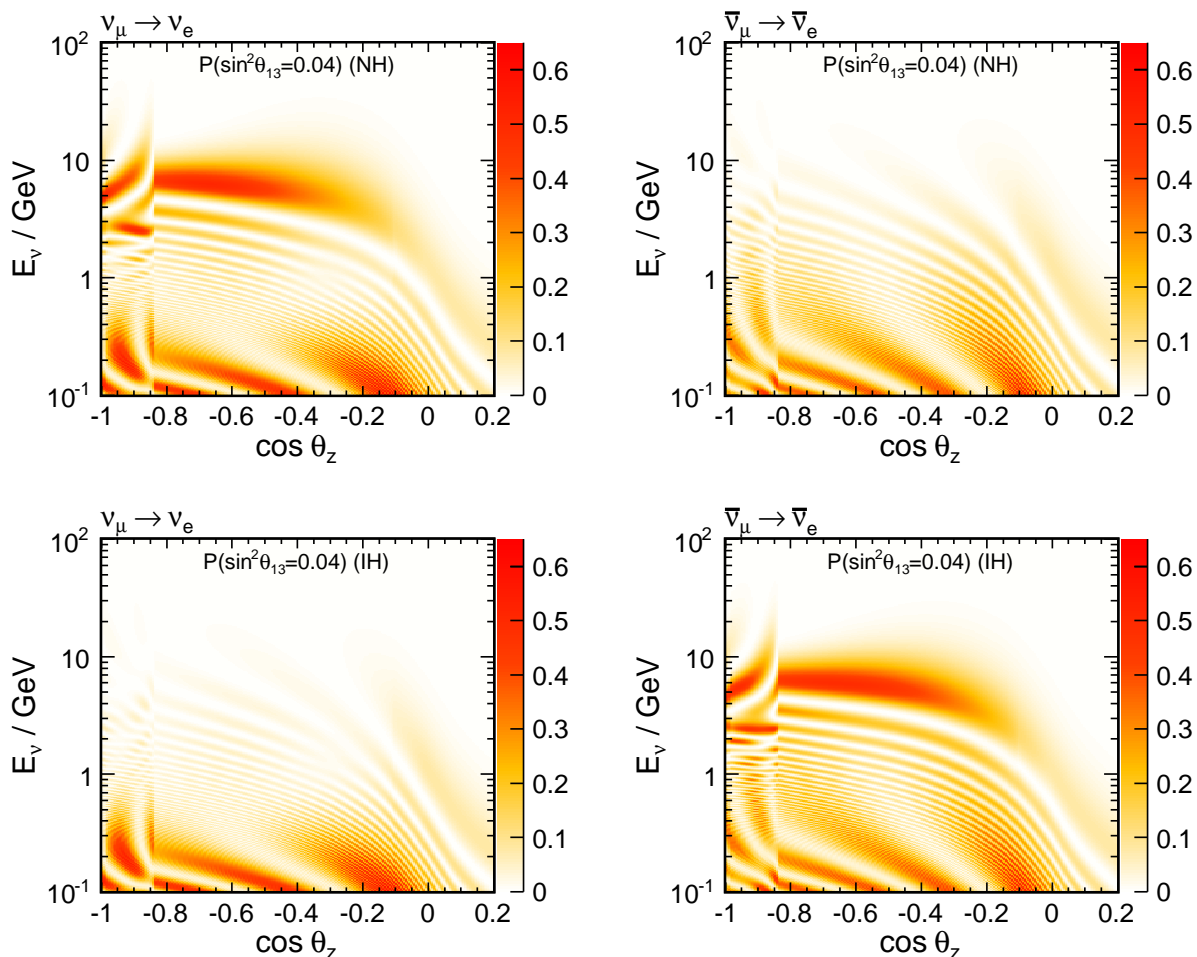


**Figure 6–24:** Atmospheric  $\nu_\mu \rightarrow \nu_e$  oscillations vs energy and zenith angle for normal hierarchy (top) and inverted hierarchy (bottom). The z axis is the oscillation probability for  $\sin^2 \theta_{13} = 0.04$ .  
**[LABEL: “fig:atnu\_osc”]**

1 the atmospheric neutrino analysis. The excellent CC/NC separation and the ability to fully  
 2 reconstruct the hadronic final state in CC interactions in a LAr-TPC would enable the  
 3 atmospheric neutrino 4-momentum to be fully reconstructed. This would enable a higher  
 4 resolution measurement of  $L/E$  to be extracted from atmospheric neutrino events in a LAr-  
 5 TPC compared to the measurements obtained from Super-Kamiokande. Using the expected  
 6 range of performance parameters for the LBNE LAr-TPC as summarized in Table 6–2,  
 7 the zenith angle distribution of atmospheric neutrinos of different flavors in a 17kt fiducial  
 8 LAr-FD module and 5 yrs of running is shown in Figure 6–25. The atmospheric neutrino  
 9 flux obtained from the Bartol model as shown in Figure 6–23, and the GENIE cross-sections  
 10 on a LAr target are used model atmospheric neutrino interactions in the LBNE LAr-FD.  
 11 The expected interaction rate is 285 events per kton-year.

12 LBNE will be able to resolve the mass hierarchy using atmospheric neutrinos alone with

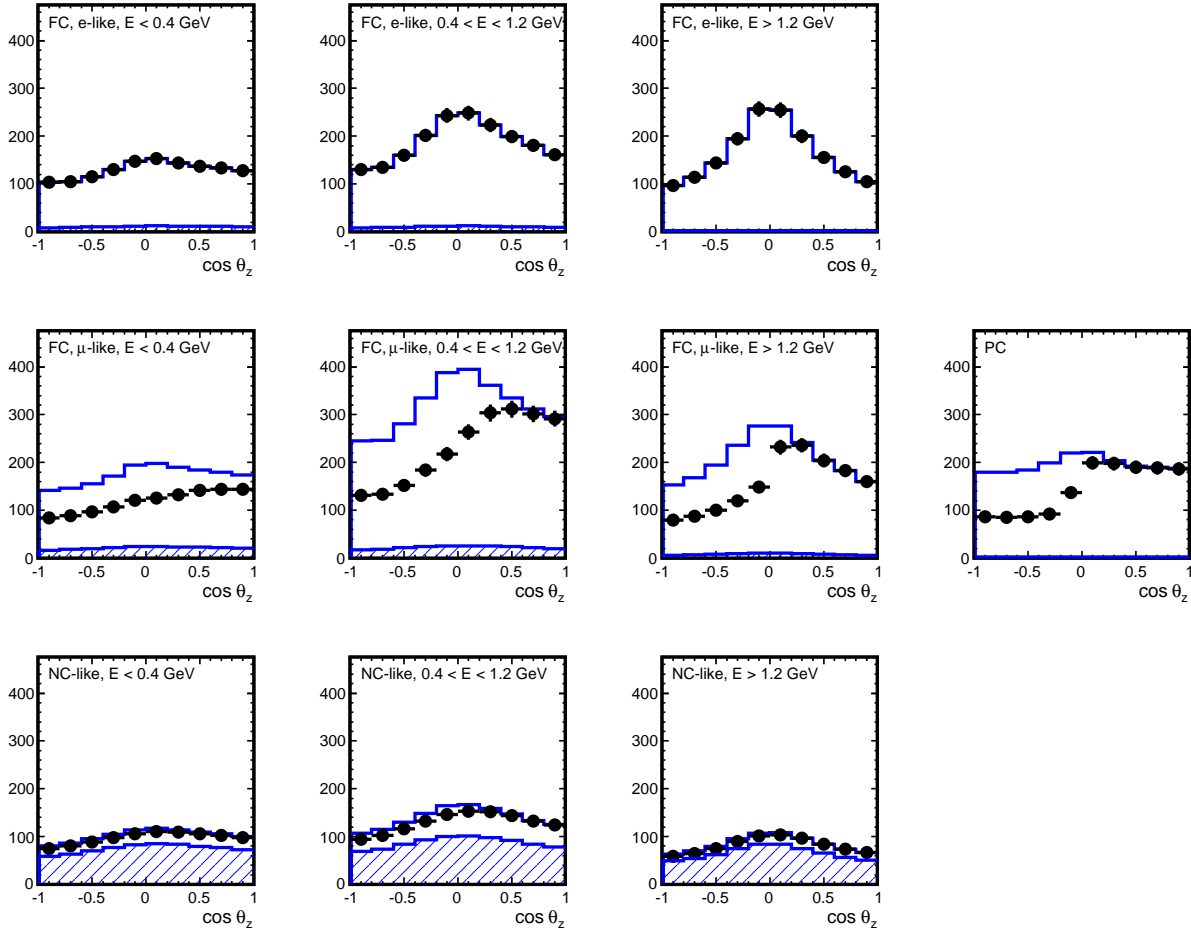


**Figure 6–25:** Zenith angle distribution for LBNE atmospheric neutrinos in a LAr-TPC with a mass of 20 kt (17 kt fiducial) and an exposure of 5 years. The solid line is for no oscillations, the hatched region is the true NC component, and the points are the oscillated expectation with some Poisson error bars added. The top set of plots is for  $\nu_e$  CC interactions, the middle plots are for  $\nu_\mu$  CC interactions and the bottom set of plots are for NC interactions. The events are divided into several energy bins as well as identified by containment: fully contained (FC) and partially contained (PC).

[LABEL: “fig:atnu\_zenith”]

- 1  $> 99\%$  C.L. after 10 yrs of running with a 34 kt fiducial LAr-TPC for values of  $\sin^2 \theta_{13} > 0.03$ .
- 2 In addition, atmospheric neutrinos provide an independent constraint on the  $\theta_{23}$  octant from
- 3 the sub-dominant oscillation at the solar mass scale - regardless of the value of  $\theta_{13}$ . The
- 4 sensitivities to the mass hierarchy and the octant of  $\theta_{23}$  obtained from atmospheric neutrinos
- 5 alone are shown in Figure 6–26.
- 6 In addition to the oscillation studies of atmospheric  $\nu_\mu, \nu_e$  CC and  $\nu$  NC, a 34-kT LAr-FD
- 7 will observe a significant excess of  $\nu_\tau$  CC events. A set of simple cuts on visible energy, re-

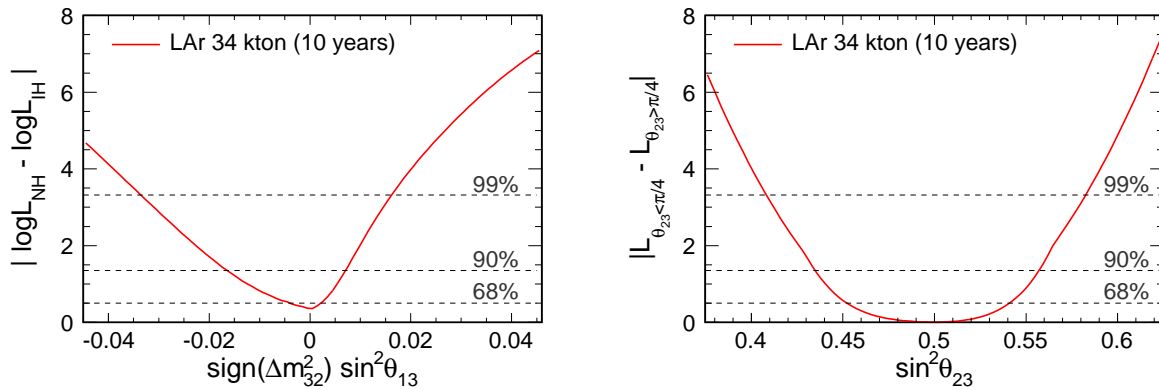


**Figure 6–26:** Sensitivities to the mass hierarchy as a function of the value of  $\sin^2\theta_{13}$  (left) and the  $\theta_{23}$  octant (right) from atmospheric neutrinos in a LAr-TPC with 34 kt fiducial mass and 10 yrs of running. These sensitivities are estimated using statistical uncertainties only.

[LABEL: “fig:atnu\_sens”]

1 construction zenith angle and energy of the highest energy pion in events lacking a charged  
 2 lepton, a  $4.3\text{-}\sigma$  excess over background can be identified in a 100 kt-yr exposure [?]. Confir-  
 3 mation of the appearance of tau neutrinos at the expected level in the atmospheric neutrino  
 4 flux as well as in the beam neutrinos will be an important consistency check on our overall  
 5 oscillation picture.

## 6.6 Accelerator-based Short-Baseline Neutrino Oscillations

7 The primary purpose of the LBNE near detector (ND) is to minimize systematic uncertainties  
 8 present in the analysis of the far detector data and provide a detailed prediction of the un-  
 9 oscillated neutrino flux measurement at the far detector. In CDR Volume 3 chapter 4, the  
 10 strategy with which to carry out such measurements is discussed. There are currently two  
 11 proposed designs for the LBNE ND, a liquid argon TPC Tracker (TPCT) and a Fine-Grained  
 12 Tracker (FGT).

13 The two ND designs under consideration are very high resolution detectors that are placed  
 14 in a short baseline high intensity neutrino beam. The LBNE ND is coupled with a next  
 15 generation instrumentation of the neutrino beam-line (Volume 3 chapter 3) that would enable  
 16 an independent measurement of the neutrino flux expected at the ND. The combination of  
 17 neutrino beam-line measurements, high intensity beam and high resolution neutrino detectors  
 18 enables the ND complex to carry out a rich program of short baseline neutrino physics.  
 19 Estimated  $\nu_\mu$  production rates on Ar at the near detector location are shown in 6–8.

20 A summary of possible physics measurements that could be achieved by the LBNE ND is  
 21 discussed here. More details on the LBNE short baseline physics program can be found in

Production mode	Rate/ton of Ar
CC QE ( $\nu_\mu n \rightarrow \mu^- p$ )	50K
NC elastic ( $\nu_\mu N \rightarrow \nu_\mu N$ )	18K
CC resonant $\pi^+$ ( $\nu_\mu N \rightarrow \mu^- N \pi^+$ )	68K
CC resonant $\pi^0$ ( $\nu_\mu n \rightarrow \mu^- p \pi^0$ )	16K
NC resonant $\pi^0$ ( $\nu_\mu N \rightarrow \nu_\mu N \pi^0$ )	16K
NC resonant $\pi^+$ ( $\nu_\mu p \rightarrow \nu_\mu n \pi^+$ )	6.9K
NC resonant $\pi^-$ ( $\nu_\mu n \rightarrow \nu_\mu p \pi^-$ )	6.0K
CC DIS ( $\nu_\mu N \rightarrow \mu^- X, W > 2$ )	69K
NC DIS ( $\nu_\mu N \rightarrow \nu_\mu X, W > 2$ )	24K
CC coherent $\pi^+$ ( $\nu_\mu A \rightarrow \mu^- A \pi^+$ )	3.9K
NC coherent $\pi^0$ ( $\nu_\mu A \rightarrow \nu_\mu A \pi^0$ )	2.0K
NC resonant radiative decay ( $N^* \rightarrow N \gamma$ )	0.11K
Inverse Muon Decay ( $\nu_\mu e \rightarrow \mu^- \nu_e$ )	12
$\nu_\mu e^- \rightarrow \nu_\mu e^-$	29
Other	42.6K
Total CC	236K
Total NC+CC	322K

**Table 6–8:** Estimated  $\nu_\mu$  production rates water an argon target per ton for  $1 \times 10^{20}$  POT at 459 m assuming neutrino cross section predictions from NUANCE [3] and a 120 GeV proton beam, 250 kA horn current, and a 2 m radius 250 m long decay region. Processes are defined at the initial neutrino interaction vertex and thus do not include final state effects. These estimates do not include detector efficiencies or acceptance [4,5].

[LABEL: “tab:nd\_rates”]

- 1 the Fall 2010 Report from the LBNE Physics Working Group [9].
- 2 The FGT is composed of straw tube tracker (STT), with transition-radiation detection ca-
- 3 pability, surrounded by a  $4\pi$  electromagnetic calorimeter, inside a dipole magnetic field of
- 4  $\mathbf{B} \approx 0.4$  T. The tracker, which also serves as the neutrino-target, has the density of liquid
- 5 hydrogen,  $\rho \approx 0.1$  gm/cm<sup>3</sup>, with a nominal fiducial mass of 7 tons. At the upstream end,
- 6 the tracker will have sufficient argon-gas, in pressurized tubes, to provide 50–100k neutrino
- 7 interactions, that is 5–10 times the statistics expected in the far LAr-detector. Detectors to
- 8 identify muons are placed within the magnet yoke as well as at downstream, and outside, of
- 9 the magnet. There is currently no detailed GEANT simulation of the ND FGT. However,
- 10 the sensitivity to different measurements is based on the performance and results achieved
- 11 by NOMAD [36] which forms the basis for the straw tube option (HiResM $\nu$ ) of the FGT.
- 12 The sensitivity studies assume a 5-year running period for neutrinos and antineutrinos with
- 13 The ND TPCT performance parameters are assumed to be similar to the LAr-TPC far de-
- 14 tector. A list of the short baseline neutrino measurements that could be carried out at the
- 15 ND complex is below

**Absoute Flux Determination** Because the flux of neutrinos — both for signal and for background — is different at ND and FD, to conduct precise measurements of  $\nu_\mu \rightarrow \nu_\tau$  oscillations, one needs to know the absolute neutrino cross-section, and hence, absolute neutrino flux, to about 3–5% precision in  $0.5 \leq E_\nu \leq 10$  GeV. Besides, absolute flux is necessary for precision measurement. The ND-FGT provides two independent, in situ determination of the absolute  $\nu_\mu$  flux.

The first method uses the elastic  $\nu$ -electron NC scattering whose cross-section is known to  $\simeq 1\%$  precision. The signal is characterized by a single  $e^-$  collinear with the beam. The background, dominated by quasi-exclusive  $\pi^0$ , where one of the photons converts asymmetrically and other evades detection, is charge symmetric. The sensitivity calculation shows that in FGT has a high efficiency for the signal ( $\approx 65\%$ ) while the background is quite benign. Furthermore, since FGT can measure  $e^-$  and  $e^+$  with equal efficiencies, any residual background can be measured. The known cross-section and the  $\nu$ -e NC events then yield an absolute measure of the neutrino flux in the  $0.5 \leq E_\nu \leq 10$  GeV range to  $\simeq 2.5\%$  precision over a 5-year running. The second method uses the ‘inverse muon decay’ (IMD) signal,  $\nu_\mu e^- \rightarrow \mu^- \nu_e$ , with a very known cross-section, to determine the absolute flux in  $E_\nu \geq 11$  GeV region. Both methods are statistics limited.

**Electro-weak Physics** A measurement of the weak mixing angle (WMA),  $\sin^2\theta_W$ , with a precision approaching 0.2% remains a prized-jewel for any short baseline neutrino program. Two independent methods of WMA determination have been explored with the FGT, each with its own caveat.

The first method uses the deep inelastic (anti)neutrino-nucleon NC and CC interactions with hadronic energy,  $E_{HAD}$ , greater than 3 GeV. NuTeV has conducted the most precise determination of WMA which, however, is  $3\sigma$  away from the expected value. The advantages of FGT over NuTeV are that in FGT (a) NC is identified as an event with no-muon *and* having a large missing transverse momentum (Pt); (b)  $\nu_e$  and  $\bar{\nu}_e$  are essentially not a background, (c) vertex resolution is much, much better than a calorimetric detector. The disadvantage of FGT over NuTeV is the lower neutrino energy. Still, there will be over  $3 \times 10^6$  ( $1.5 \times 10^6$ ) NC events in FGT in a 5-year  $\nu(\bar{\nu})$  running, providing sufficient statistics to measure WMA to about 0.11% precision. Preliminary investigations suggest that systematics due to charm, strange-sea and the longitudinal structure functions can be controlled at 0.2% precision. Importantly, over the life-time of LBNE, we will have a high-energy run providing a highly-redundant and systematically independent checks of oscillation phenomena. A high-energy run will also furnish a higher-energy spectrum for WMA analysis.

The second method uses the elastic  $\nu_\mu$ -electron and  $\bar{\nu}$ -electron NC scattering. The systematic advantage of FGT over the CHARM-II measurement is manifest. However, given the light FGT mass, the statistics of these interactions is insufficient. However, if the ND-complex uses a several-hundred ton LAr (e.g. LAr1) followed by FGT — a choice which will provide the best systematic constraints on errors associated with oscillation — then there will be sufficient statistics to conduct a 0.5% measurement of

1 WMA using neutrino-electron.

2 Given the importance of WMA, and an alive  $3\sigma$  anomaly, the quest for WMA remains  
3 an attractive goal.

4 **Structure of the Weak Current** FGT provides a unique matrix of measurements to explore  
5 the structure of the weak current. Using the Coherent  $\pi^0$ ,  $\pi^+$ , and  $\pi^-$  interactions,  
6 the partially conserved vector current (PCAC) and the low- $Q^2$  structure of the weak  
7 current can be explored. The coherent-pion have a clean signature in FGT where the  
8 backgrounds from QE, resonance, and DIS channels can be controlled to precision much  
9 better than any experiment (including currently envisioned). Using the Coherent  $\rho^0$ ,  
10  $\rho^+$ , and  $\rho^-$  interactions, the conserved vector current (CVC) and the vector-hadron  
11 dominance (VMD) of the weak current can be explored. The coherent- $\rho^+/\rho^-$  have  
12 been observed at  $\simeq 3\sigma$  level, but coherent- $\rho^0$  has not been observed. The resolution  
13 of FGT and the intensity of the LBNE beam makes it possible to conduct these 6  
14 measurements precisely and elucidate the weak current with a clarity that has never  
15 been attempted.

16 **Other Precision Measurements** Among other sensitivity studies, conducted by the LBNE  
17 Short-Baseline Physics (SBP) group, are included topics like strange content of the  
18 nucleon, structure functions, perturbative versus non-perturbative QCD, strange meson  
19 and baryon production, and sum-rules. These will be duly summarized in the report  
20 by the Physics Working Group (PWG). In the following, two searches at the ND are  
21 mentioned.

22 **High  $\Delta m^2$  Neutrino Oscillations** The FGT's ability to measure all four species of CC in-  
23 teractions,  $\nu_{\mu^-}$ ,  $\bar{\nu}_{\mu^-}$ ,  $\nu_{e^-}$  and  $\bar{\nu}_{e^-}$ -CC, permits a sensitive search for  $\nu_{\mu} \rightarrow \nu_e$  transition,  
24 or, equivalently, oscillation with high- $\Delta m^2$  ( $\geq 1\text{eV}^2$ ). Using  $\nu_{\mu^-}$  and  $\bar{\nu}_{\mu^-}$ -CC events,  
25 the electron-neutrino yields from  $\mu$  and charged-kaons in the beam can be determined  
26 to a high precision. (Both NOMAD and NuTeV used this method to constrain the  $\nu_e$   
27 content of the beam.) Additionally, the  $K_L^0$  component can be uniquely determined us-  
28 ing the small anti- $\nu_e$  in the beam. Finally, the non-prompt background (dominated by  
29 NC) can be measured using kinematic variables in the plane transverse to the neutrino-  
30 direction. Preliminary studies suggest that the probability of  $\nu_{\mu} \rightarrow \nu_e$  transition can  
31 be explored with a sensitivity of  $10^{-4}$ , i.e. an order of magnitude better precision than  
32 currently available. We point out that external hadro-production measurements of the  
33 ratios of  $K^+/\pi^+$ ,  $K^-/\pi^-$  and  $K^0/K^+$  will immensely help this search and aid the  
34 simulation of the LBNE beam.

35 Finally, the NOMAD experiment conducted a search of  $\nu_{\mu} \rightarrow \nu_{\tau}$  transition with  
36 a probability of  $10^{-4}$ . The search of  $\tau$ -appearance was done using the existence of  
37 missing-Pt in the non-muonic decay modes, while using the  $\nu_{\mu}$ -CC as a control sam-  
38 ple. The search-sensitivity was dominated by channels with  $\leq 0.1$ -event backgrounds.  
39 At LBNE, the strengths of FGT over NOMAD are (a) higher-resolution and a more  
40 hermetic detector, and (b) much higher intensity; the weakness is the lower-energy im-  
41 plying a higher threshold. But in a high energy-run (see above), the FGT should be

1 able to conduct the  $\nu_\mu \rightarrow \nu_\tau$  transition with an order of higher sensitivity.

## 2 6.7 Summary of Expected Measurements in LBNE

Parameter	Resolution/Sensitivity
$\nu_\mu \rightarrow \nu_e$ CC	
Sign $\Delta m_{31}^2$ $\delta_{CP} \neq 0, \pi$ $\sin^2 2\theta_{13} = 0.1$ $\delta_{CP} = 0$ Determination of $\theta_{23}$ quadrant Non standard interactions	$> 5\sigma$ for all values of $\delta_{CP}$ $> 3/5\sigma$ for 65%/40% of $\delta_{CP}$ values $\sigma(\sin^2 2\theta_{13}) = 0.005$ $\sigma(\delta_{CP}) = 18^\circ$ $> 90\%$ C.L. for $\theta_{23} < 42^\circ$ and $\theta_{23} > 49^\circ$ Figure 6-17
$\nu_\mu \rightarrow \nu_\mu$ CC	
$\sin^2 2\theta_{23} = 1.0$ ( $\nu$ ) $\Delta m_{32}^2 = 2.4 \times 10^{-3} \text{ eV}^2$ ( $\nu$ ) $\sin^2 2\theta_{23} = 1.0$ ( $\bar{\nu}$ ) $\Delta m_{32}^2 = 2.4 \times 10^{-3} \text{ eV}^2$ ( $\bar{\nu}$ ) Non standard interactions Long range interactions $\alpha$	$\sigma = 0.007$ $\sigma = 0.017 \times 10^{-3} \text{ eV}^2$ $\sigma = 0.011$ $\sigma = 0.025 \times 10^{-3} \text{ eV}^2$ Figure 6-17 ongoing studies
$\nu \rightarrow \nu$ NC	
Sterile fraction, $f_s$ Non-standard interactions	ongoing studies ongoing studies
$\nu_\mu \rightarrow \nu_\tau$ CC	
$\nu_\tau$ appearance	ongoing studies

**Table 6-9:** Expected measurement precision/sensitivities of long-baseline  $\nu_\mu$  oscillation parameters in LBNE assuming an exposure of 34 kt LAr, 5+5 years  $\nu + \bar{\nu}$  running at 708 kW. Values are quoted assuming a normal mass hierarchy.

[LABEL: "table:lbl\_conclusions\_resolution\_app"]

Parameter	Resolution/Sensitivity
Absolute Flux	2.5-3%
$\sin^2 \theta_W$ using $\nu$ -q	→ 0.25%
$\sin^2 \theta_W$ using $\nu$ -e	→ 0.5%
$P(\nu_\mu \rightarrow \nu_e) (\Delta m^2 \geq 1 \text{ eV}^2)$	→ $10^{-4}$
$P(\nu_\mu \rightarrow \nu_\tau) (\Delta m^2 \geq 1 \text{ eV}^2)$	→ $10^{-5}$
PCAC (Coherent- $\pi^0, \pi^+, \pi^-$ )	OK
CVC/VMD (Coherent- $\rho^0, \rho^+, \rho^-$ )	OK

**Table 6-10:** Expected measurement precision/sensitivities using short-baseline  $\nu_\mu$  interactions in the NDC, with an LAr and a 7 t FGT, assuming an exposure of 5+5 years  $\nu + \bar{\nu}$  running at 708 kW.

[LABEL: “table:sbl\_conclusions\_resolution\_app”]

## 7 Supporting Documents

[LABEL: “v1ch-supp-doc”]

A host of information related to the CDR is available in a set of supporting documents. Detailed information on risk analysis and mitigation, value engineering, ES&H, costing, project management and other topics not directly in the design scope can be found in these documents, listed in Table 7-1. Each document is numbered and stored in LBNE’s document database, called DocDB, accessible via a username/password combination provided by the Project. Project documents stored in DocDB are also made available to internal and external review committees through Web sites developed to support individual reviews.

**Table 7-1: LBNE CD-1 Documents** [LABEL: “table:cd-1-doc-list”]

Title	DocDB Number(s)
Acquisition Plan (AP)	5329
Alternatives Analysis	4382
Case Study Report; Liquid Argon TPC Detector	3600
Configuration Management Plan	5452
DOE Acquisition Strategy for LBNE	5442
Environment, Safety and Health (ES&H) Plan	4514
LAr-FD Preliminary ODH Analysis	2478
Global Science Objectives, Science Requirements and Traceback Reports	4772
Preliminary Hazard Analysis Report	4513
Preliminary Project Execution Plan	5443
Project Management Plan (PMP)	2453
Project Organization Chart	5449
Quality Assurance Plan (QAP)	2449
Report on the Depth Requirements for a Massive Detector at Homestake	0034
Requirements, Beamline	4835
Requirements (Parameter Tables), Far Detector	3747 (2843)

Requirements, Far Site Conventional Facilities	4408
Requirements, Near Detectors	5579
Requirements, Near Site Conventional Facilities	5437
Risk Management Plan (RMP) and Risk Register	2445
Value Engineering Report	3082
Work Breakdown Structure (WBS)	4219



## References

- [1] S.Amoruso *et al.* *Eur. Phys. J.*, vol. C33, p. 233, 2004.
- [2] A.Bueno *et al.* *JHEP*, vol. 0704, p. 041, 2007.
- [3] D. Casper, “The nuance neutrino physics simulation, and the future.,” *Nucl.Phys.Proc.Suppl.*, vol. 112, p. 161, 2002.
- [4] tech. rep. LBNE-doc-740.
- [5] tech. rep. LBNE-doc-783.
- [6] LBNE Science Collaboration, LBNE Case Study Report, Liquid Argon TPC Far Detector, Draft Version 1.2, October 2, 2011.
- [7] Particle Physics Project Prioritization Panel, “US Particle Physics: Scientific Opportunities; A Strategic Plan for the Next Ten Years,” 2008. [http://science.energy.gov/~media/hep/pdf/files/pdfs/p5\\_report\\_06022008.pdf](http://science.energy.gov/~media/hep/pdf/files/pdfs/p5_report_06022008.pdf).
- [8] LBNE Project Office, “LBNE Project Management Plan,” tech. rep., FNAL, 2011. LBNE DocDB 2453.
- [9] T. Akiri *et al.*, “The 2010 Interim Report of the Long-Baseline Neutrino Experiment Collaboration Physics Working Groups.” arXiv:1110.6249.
- [10] “LBNE Liquid Argon TPC Detector Case Study,” tech. rep. LBNE-doc-3600.
- [11] A. Bernstein *et al.*, “Report on the Depth Requirements for a Massive Detector at Home-stake (LBNE-doc-34),” 2008. FNAL-TM-2424-E, BNL-81896-2008-IR, arXiv:0907.4183.
- [12] “A Proposal for a Detector 2 km Away from the T2K Neutrino Source,” 2005. <http://www.phy.duke.edu/~cwalter/nusag-members/2km-proposal-05-05-30.pdf>.
- [13] “A Large Liquid Argon Time Projection Chamber for Long-baseline Off-Axis Neutrino Oscillation Physics with the NuMI Beam,” tech. rep., 2005. Submitted to the NuSAG committee; inspirehep.net FERMILAB-FN-0776-E.
- [14] tech. rep. LBNE-doc-266-v1, LBNE-doc-3414-v2.

- 1 [15] tech. rep. LBNE-doc-5446.
- 2 [16] P. Adamson *et al.*, “Improved search for muon-neutrino to electron-neutrino oscillations  
3 in MINOS,” *Phys. Rev. Lett.*, vol. 107, p. 181802.
- 4 [17] A. Ankowski *et al.* *Eur. Phys. J.*, vol. C48, p. 667, 2006.
- 5 [18] W. A. Mann *et al.*, “Apparent multiple  $\Delta m_{32}^2$  in muon anti-neutrino and muon neutrino  
6 survival oscillations from non-standard interaction matter effect,” *Phys. Rev. D.*, vol. 82,  
7 p. 113010, 2010.
- 8 [19] U. Kose, “Search for  $\nu_{\mu} \rightarrow \nu_{\tau}$  oscillations in appearance mode in the OPERA experi-  
9 ment..” arXiv:1106.3871 [hep-ex], 2011.
- 10 [20] P. Adamson *et al.*, “Search for the disappearance of muon antineutrinos in the NuMI  
11 neutrino beam,” *Phys. Rev. D.*, vol. 84, p. 071103, 2011. arXiv:1108.1509 [hep-ex].
- 12 [21] J. Kopp arXiv:1010.3706.
- 13 [22] S. Davidson, C. Pena-Garay, N. Rius, and A. Santamaria hep-ph/0302093, 2003.
- 14 [23] M.C. Gonzalez-Garcia, and M. Maltoni *Phys. Rept.*, vol. 460, p. 1, 2008. arXiv:0704.1800  
15 [hep-ph].
- 16 [24]
- 17 [25] “The LArSoft Collaboration.” [https://plone4.fnal.gov:4430/P1/Main/wiki/  
18 LArSoft/LArSoft.](https://plone4.fnal.gov:4430/P1/Main/wiki/LArSoft/LArSoft)
- 19 [26] T.Totani *et al.*, “Future detection of supernova neutrino burst and explosion mecha-  
20 nism,” *Astrophys. J.*, vol. 496, p. 216, 1998.
- 21 [27] S. Coleman and S. Glashow *Phys. Rev. Lett.*, vol. B405, p. 249, 1997.
- 22 [28] F. Klinkhamer and G. Volovik *Intl. Jour. of Mod. Phys.*, vol. A20, p. 2795, 2005.
- 23 [29] D. Colladay and V. Kostelecky *Phys. Rev. D.*, p. 116002, 1998.
- 24 [30] Y. Grossman *et al.* *Phys. Rev. D.*, vol. 72, p. 125001, 2005.
- 25 [31] M. C. Gonzalez-Garcia *et al.* *Nucl. Phys. B*, vol. 573, p. 3, 2000.
- 26 [32] D. Kaplan *et al.* *Phys. Rev. Lett.*, vol. 93, p. 091801, 2004.
- 27 [33] K. Abe *et al.* *Phys. Rev. D*, vol. 77, p. 052001, 2008.
- 28 [34] W. Wang. PhD thesis, 2007.
- 29 [35] G. Mitsuka, *Study of Non-Standard Neutrino Interactions with Atmospheric Neutrino  
30 Data in Super-Kamiokande.* PhD thesis, University of Tokyo, 2009.

- 
- <sup>1</sup> [36] J. Altegoer *et al.*, “The nomad experiment at the cern sps,” *Nucl. Instrum. Meth.*,  
<sup>2</sup> vol. A404, p. 96, 1998.